Gulf of Mexico Offshore Wind Energy Hurricane Risk Assessment

Lauren A. Mudd and Peter J. Vickery

Applied Research Associates, Inc.

NREL Technical Monitor: Rebecca Fuchs

NREL is a national laboratory of the U.S. Department of Energy
Office of Energy Efficiency & Renewable Energy
Operated by the Alliance for Sustainable Energy, LLC

This report is available at no cost from the National Renewable Energy Laboratory (NREL) at www.nrel.gov/publications.

Contract No. DE-AC36-08GO28308

Subcontract Report
NREL/SR-5000-88211
December 2023

Gulf of Mexico Offshore Wind Energy Hurricane Risk Assessment

Lauren A. Mudd and Peter J. Vickery

Applied Research Associates, Inc.

NREL Technical Monitor: Rebecca Fuchs

Suggested Citation
Mudd, Lauren A., and Peter J. Vickery. 2023. *Gulf of Mexico Offshore Wind Energy Hurricane Risk Assessment*. Golden, CO: National Renewable Energy Laboratory. NREL/SR-5000-88211. https://www.nrel.gov/docs/fy24osti/88211.pdf.

NREL is a national laboratory of the U.S. Department of Energy
Office of Energy Efficiency & Renewable Energy
Operated by the Alliance for Sustainable Energy, LLC

This report is available at no cost from the National Renewable Energy Laboratory (NREL) at www.nrel.gov/publications.

Contract No. DE-AC36-08GO28308

Subcontract Report
NREL/SR-5000-88211
December 2023

National Renewable Energy Laboratory
15013 Denver West Parkway
Golden, CO 80401
303-275-3000 • www.nrel.gov

NOTICE

This work was authored in part by the National Renewable Energy Laboratory, operated by Alliance for Sustainable Energy, LLC, for the U.S. Department of Energy (DOE) under Contract No. DE-AC36-08GO28308. Funding provided by the U.S. Department of Energy Office of Energy Efficiency and Renewable Energy Wind Energy Technologies Office. The views expressed herein do not necessarily represent the views of the DOE or the U.S. Government.

Cover Photos by Dennis Schroeder: (clockwise, left to right) NREL 51934, NREL 45897, NREL 42160, NREL 45891, NREL 48097, NREL 46526.

Acknowledgments

The authors would like to thank the following reviewers and contributors from the National Renewable Energy Laboratory (NREL): Becca Fuchs and Walt Musial.

This report was funded under a subcontract between Applied Research Associates, Inc. and NREL, through an interagency agreement between the U.S. Department of Energy's National Renewable Energy Laboratory and the Department of the Interior's Bureau of Ocean Energy Management in the Gulf of Mexico region. The authors would like to extend thanks to Tershara Matthews, Dr. Jim Kendall, Mike Celata, Idrissa Boube, Lenny Coats and Bridgette Duplantis from the Bureau of Ocean Energy Management Gulf of Mexico for their leadership and support for this research.

This report was peer reviewed by Jiali Wang from Argonne National Laboratory and Murray Fisher from Gulf Wind Technology.

In addition, we would like to acknowledge the technical project management support from NREL staff including Setareh Saadat and Betsy Sara and document editing by Emily Horvath and Sheri Anstedt.

List of Acronyms

ASCE	American Society of Civil Engineers
CDF	cumulative distribution function
C-MAN	Coastal-Marine Automated Network
ESDU	Engineering Sciences Data Unit
GPS	Global Positioning System
HURDAT2	Atlantic Basin Best Track Data
IEC	International Electrotechnical Commission
km	kilometer
mph	miles per hour
m/s	meters per second
m	meter
NCAR	National Center for Atmospheric Research
NOAA	National Oceanic and Atmospheric Administration
NREL	National Renewable Energy Laboratory
RMW	radius of maximum wind
RP	return period
SST	sea surface temperature

List of Symbols

B	Holland B parameter
c	translation speed of the tropical cyclone
C_d	drag coefficient
C_p	phase speed of waves
f	Coriolis parameter
g	acceleration due to gravity
H	boundary layer height
I	relative intensity
k	von Karmen constant
p	pressure
r	radial distance
R^2	coefficient of determination
R_B	wind-sea Reynolds number
R_d	gas constant for dry air
RMW	radius of maximum wind
T	duration the wind blows over a fetch of length χ
T_o	tropopause temperature
T_s	significant wave period
U	mean wind speed
$u*$	friction velocity
U_h	translation speed of the tropical cyclone
V_g	gradient wind speed
V_s	scaled vertical wind shear
z	height
z_0	surface roughness
B	wave age
δ	angle between the mean wind speed and the surface waves
ε	error term
θ	storm heading of tropical cyclone
λ	occurrence rate
ρ_a	density of air
ρ_w	density of sea water
τ_0	surface shear stress
υ	kinematic viscosity of sea water
Υ	longitude
Ψ	latitude

Executive Summary

The National Renewable Energy Laboratory's (NREL's) feasibility assessment of offshore wind in the Gulf of Mexico concluded that hurricane risk was one of the major challenges that would need to be overcome for a mature offshore wind industry to develop in the Gulf of Mexico (Musial and Greco 2020). To ensure the robust design of wind turbines in the Gulf of Mexico, it is critical to understand the added risk posed by the threat of major hurricanes because those affecting the Gulf of Mexico region have a significant potential to exceed design limits prescribed by the International Electrotechnical Commission (IEC) wind design standards.

NREL was contracted under an Interagency Agreement with the Bureau of Ocean Energy Management's Gulf of Mexico region to examine the economic, geographical, and technical challenges of potential offshore wind development in the Gulf of Mexico (Fuchs et al. 2023). Under subcontract to NREL, Applied Research Associates, Inc. was hired to examine the hurricane risk to wind turbines operating in the region—a harmonization between the terminology used by the National Hurricane Center and the IEC, which writes the standards used for wind turbine design, and a geospatial assessment of the risk to IEC class turbines.

To satisfy this charge, this project defines the wind hazard for the Gulf of Mexico Offshore Wind Energy Call Area using the hurricane hazard model developed by Applied Research Associates and published extensively in the open literature. In doing so, the return periods associated with the IEC Class 1A and Typhoon Class limit-state hurricanes are estimated on a grid with nominal resolution of 10 kilometers (km) to determine where hurricane risk results in the exceedance of the IEC design criteria. On the same grid, wind speed hazard contours associated with return periods varying from 50 to 1,000 years are also estimated.

An additional challenge in assessing hurricane wind speed risk in the Gulf of Mexico arises from inconsistent terminology across the Saffir-Simpson hurricane scale and the IEC design criteria. Saffir-Simpson definitions are based on 1-minute sustained wind speeds estimated at 10-meter (m) height over marine terrain, while the IEC uses a different averaging period (3-second versus 1-minute) and reference height (assumed herein a hub height of 150 m versus 10 m). Employing the latest research on turbulence characteristics of the hurricane boundary layer, conversions between various durations (e.g., 3 seconds, 1 minute, 10 minutes, 1 hour) and between elevations near the surface (10 m) to near hub height (assumed herein 150 m) are developed. IEC Class 1A and Typhoon Class limit states are also provided in terms of an equivalent Saffir-Simpson hurricane wind speed category.

The following sections describe the hurricane hazard model and analysis methodology (Section 1) and present harmonized hurricane terminology for offshore wind design (Section 2) and the results of the hurricane risk assessment for the Gulf of Mexico offshore resource area (Sections 3 and 4).

Table of Contents

List of Figures

List of Tables

1 Hurricane Hazard Model

The key components of the hurricane hazard model are i) probabilistic models describing the occurrence rates, storm tracks, and intensities (Vickery et al. 2009b) and ii) the hurricane wind field model (Vickery et al. 2009a).

1.1 Hurricane Track and Intensity Modeling

The probabilistic portion of the hurricane hazard model is described in detail in Vickery et al. (2000b, 2009b). The key features of the storm track model are the coupling of the modeling of the central pressure with sea surface temperature (SST) and the ability to model curved tracks that can make multiple landfalls. The entire track of a storm is modeled, from the time of storm initiation over the water until the storm dissipates. The starting times (hour, day, and month) and locations of the storms are taken directly from the Atlantic Basin Best Track Data, hereafter HURDAT2 (Landsea and Franklin 2013). Using the actual starting times and locations ensures that any climatological preference for storms to initiate in different parts of the Atlantic Basin at different times of the year is maintained.

The coupling of the central pressure modeling to sea surface temperature ensures that intense storms (such as Category 5 storms) cannot occur in regions in which they physically could not exist (such as at extreme northern latitudes). As shown in Vickery et al. (2000b, 2009b), the approach reproduces the variation in the central pressure characteristics along the United States coastline. In the hurricane hazard model, the storm's intensity is modeled as a function of the sea surface temperature and wind shear until the storm makes landfall. At the time of landfall, the filling models described in Vickery (2005) are used to exponentially decay the intensity of the storm over land. Over land, following the approach outlined in Vickery et al. (2009b), the storm size is modeled as a function of central pressure and latitude. If the storm exits land into the water, the storm intensity is again modeled as a function of sea surface temperature and wind shear, allowing the storm to possibly reintensify and make landfall again elsewhere.

The validity of the modeling approach for storms near the coastal United States is shown through comparisons of the statistics of historical and modeled key hurricane parameters along the North American coast. Comparisons of occurrence rate, heading, translation speed, distance of closest approach, and so on, are given in Vickery et al. (2009b). These comparisons are made using the statistics derived from historical and modeled storms that pass within 250 kilometers (km) of a coastal milepost location. The comparisons are also given for mileposts spaced 50 nautical miles apart along the entire United States Gulf and Atlantic coastlines. In all comparison figures in Vickery et al. (2009b), the 90% confidence bounds are also plotted and shown to encompass the historical data, indicating with 90% confidence that the historical and modeled data are from equivalent statistical distributions. Results of additional statistical testing using the chi-square, Kolmogorov-Smirnov, and James and Mason tests of equivalent distributions are also provided, indicating that the confidence in equivalent distributions of some track modeling parameters may be as high as 95%. Validation examples are also presented later in this section.

1.1.1 Hurricane Occurrence Rate and Storm Track Modeling

The number of storms to be simulated in any given year is obtained by sampling from a negative binomial distribution. The starting position, date, time, heading, translation speed, and central pressure of all tropical storms, as given in the HURDAT2 database, are sampled and used to initiate the simulation. Using the historical starting positions of the storms (i.e., date and location) ensures that the climatology associated with any seasonal preferences for the point of storm initiation is retained. Given the initial storm heading, speed, and intensity, the simulation model estimates the new position and speed of the storm based on the changes in the translation speed and storm heading over the current 6-hour period. The changes in the translation speed, c, and storm heading, θ, between times i and $i+1$ are obtained from

$$\Delta \ln c = a_1 + a_2\psi + a_3\gamma + a_4 \ln c_i + a_5\theta_i + \varepsilon \quad (1a)$$

$$\Delta\theta = b_1 + b_2\psi + b_3\gamma + b_4 c_i + b_5\theta_i + b_6\theta_{i-1} + \varepsilon \quad (1b)$$

where a_1, a_2, and so on, are constants; Ψ and γ are the storm latitude and longitude, respectively; c_i is the storm translation speed at time step i; θ_i is the storm heading at time step i; θ_{i-1} is the heading of the storm at time step $i-1$; and ε is a random error term. The coefficients a_1, a_2, and so on have been developed using 5-degree by 5-degree grids over the entire Atlantic Basin. Over much of the Atlantic Basin, a different set of coefficients for easterly and westerly headed storms is used. As the simulated storm moves into a different 5-degree by 5-degree square, the coefficients used to define the changes in heading and speed change accordingly.

1.1.2 Hurricane Intensity Modeling

Hurricane intensity, as defined by central pressure difference, is modeled as a function of the relative intensity, I, and thermodynamic and atmospheric environmental variables including SST, tropopause temperature, and vertical wind shear. The relative intensity approach is based on the efficiency of a cyclone relative to a Carnot heat engine (Emanuel 1988). The definition of the relative intensity used here is the ratio of the central pressure difference at the center of a cyclone to the maximum possible central pressure difference for the given meteorological conditions. The key parameters controlling the relative intensity are SST, tropopause temperature, T_o, and the relative humidity. Relative humidity is taken here as a constant equal to 0.8.

For each storm in the HURDAT2 database where central pressure data are available and the storm is over water, the relative intensity is computed using the central pressure difference, SST, tropopause temperature, and relative humidity (assumed constant and equal to 0.8). The SST at the storm center is determined from the Hadley Centre Sea Ice and Sea Surface Temperature dataset (Rayner et al., 2003), which provides monthly mean SSTs for the period of 1850–2019 on a 1-degree geographical grid. The T_o temperature data were obtained from the National Center for Atmospheric Research (NCAR) reanalysis database (www.cdc.noaa.gov), which provides T_o data on a 2.5-degree geographical grid. A linear two-dimensional interpolation method is used to obtain the values of SST and T_o at the storm center.

A simple one-dimensional ocean mixing model described in Emanuel et al. (2006) is used to simulate the effect of ocean feedback on the relative intensity calculations. The ocean feedback model calculates the mixed layer depth based on the assumed constancy of a bulk Richardson number, while the mixed layer momentum is driven by the surface stress and entrainment. The

mixed layer momentum equation is integrated over a circular region of 4 times the radius of maximum wind (RMW). The ocean mixing model returns an estimate of the mixed layer depth, which is then used to compute the reduction in sea surface temperature caused by the passage of a hurricane. This reduced temperature is used in the relative intensity calculations.

The relative intensity values are subsequently used to develop regional statistical models in the form of Eq. 2, where the relative intensity at any time is modeled as a function of relative intensity at the previous three steps and the scaled vertical wind shear, V_s (DeMaria and Kaplan 1999):

$$\ln(I_{i+1}) = c_1 \ln(I_i) + c_2 \ln(I_{i-1}) + c_3 \ln(I_{i-2}) + c_4 V_s + \varepsilon \quad (2)$$

where c_1, c_2, and so on are constants that vary with region in the Atlantic Basin and ε is a random error term. In the development of the dataset of historical values of I, the surface-level wind speeds required for estimating c_1, c_2, and so on for use in the ocean mixing model were obtained using the simple wind field model described in Holland (1980), with the surface-level mean wind speed equal to 80% of the gradient balance wind speed. Nine different regions are used to model the intensity changes of tropical cyclones in the Atlantic Basin.

In the simulation process, hurricanes that make landfall are weakened (filled) with the filling model as described in Vickery (2005). If the center of the hurricane reenters the water, Eq. 2 is again used to model the change in I. On the center of the hurricane first reentering the water, the values of I_{i-1}, I_{i-2}, and so on used in Eq. 2 are all set to the value computed upon reentry. Ocean mixing is computed using the same simple Holland (1980) wind model used in the model development.

Estimates of wind speeds derived using the track and intensity models are coupled with the hurricane wind field model described in Vickery et al. (2009a), statistical models for the *RMW* and Holland *B* parameter described in Vickery and Wadhera (2008), and a deterministic model used to decay the magnitude of *B* after a hurricane makes landfall. Modeling of *RMW* and of the Holland *B* parameter—which describes the pressure-wind relationship used in the wind field model as well as the overall shape of the hurricane—is described in further detail in Section 1.1.2.1. In the modeling of *RMW* and *B*, an error term is sampled prior to the start of each simulated storm and is used throughout the simulation as a shift from the mean regression model. Using this approach, a storm that starts out larger than average remains larger than average throughout its modeled life. Similarly, a storm with a sampled value of *B* that is larger or smaller than average remains larger or smaller throughout its modeled life.

1.1.3 Hurricane Track and Intensity Validation

The HURDAT2 database is used to validate the model away from the U.S. coastline. HURDAT2 contains position data (latitudes and longitudes), central pressures, and estimates of the maximum wind speed (maximum 1-minute average wind speed at a height of 10 m) given in increments of 5 knots. Prior to the satellite era (~1970), information on central pressure is limited to near-shore estimates obtained by reconnaissance aircraft. These limited aircraft data are available starting in the mid-1940s. Prior to the aircraft era, estimates of central pressure were derived from ship reports and other ground sources.

The HURDAT2 data are archived at 6-hour increments. Furthermore, central pressures other than those at the start and end of each 6-hour segment are not recorded. Therefore, it is unlikely that one these 6-hour positions contain the minimum central pressure experienced over the life of the storm.

In addition to the information obtained from the HURDAT2 dataset, the model is validated/calibrated using a separate dataset that provides details on landfall pressures (Blake et al. 2011). Both the landfall dataset and the HURDAT2 dataset are continually being updated through the ongoing HURDAT2 reanalysis project (http://www.aoml.noaa.gov/hrd/data_sub/re_anal.html). The HURDAT2 dataset used here includes all revisions to historical storm data through the June 2019 HURDAT2 update.

Figure 1 and Figure 2 present example comparisons of the modeled and historical cumulative distribution functions (CDF) of storm heading (i.e., the direction a storm is traveling) and storm translation speed (i.e., the speed at which a storm is traveling) in the Gulf of Mexico. In addition to the CDFs, Figure 1 and Figure 2 also include a simplified coastline of the western Gulf of Mexico from Mexico to Louisiana as shown by the blue line. Each CDF was developed using information on all historical tropical cyclones passing within 250 km of a specified latitude-longitude pair. These validation circles are centered on a 2-degree grid, with results presented here encompassing the western Gulf of Mexico from 22°N to 32°N latitude and 90°W to 98°W longitude.

Figure 3 presents example comparisons of modeled and observed central pressures plotted versus return period. For orientation purposes, a simplified coastline of the western Gulf of Mexico from Mexico to Louisiana is also shown by the blue line in Figure 3. The observed central pressures plotted versus return period were computed assuming that the *Np* pressure data points obtained from a total of *N* tropical cyclones that pass through the circle are representative of the full population of *N* storms. With this assumption, the CDF for the conditional distribution for storm central pressure is computed, where each pressure has a probability of 1/(*Np*+1). The return period associated with a given central pressure is obtained from

$$P_t(p_c < P_c) = 1 - \sum_{x=0}^{\infty} P_t(p_c > P_c|x)p_t(x) \tag{3}$$

where $P_t(p_c > P_c|x)$ is the probability that velocity *v* is less than *V* given that *x* storms occur, and $p_t(x)$ is the probability of *x* storms occurring during time period *t*. From Eq. 3, with $p_t(x)$ defined as Poisson and defining *t* as 1 year, the annual probability of exceeding a given wind speed is

$$P_a(p_c < P_c) = 1 - exp[-\lambda P(p_c < P_c)] \tag{4}$$

where λ is the annual occurrence rate defined as N/N_Y where N_Y is the number of years in the historical record, here equal to 120 years (1900 through 2019).

The model estimates of central pressure versus return period for a given location are computed using Eq. 4, where λ is the annual occurrence rate of simulated storms affecting the location of interest (e.g., the number of simulated storms within 250 km of a location divided by the number

of simulated years). The probability distribution for central pressure is obtained by rank ordering the simulated central pressures. The comparisons of modeled and observed central pressures given in Figure 3 use the minimum value of the central pressures while a storm (modeled or historical) is within the 250 of the indicated point.

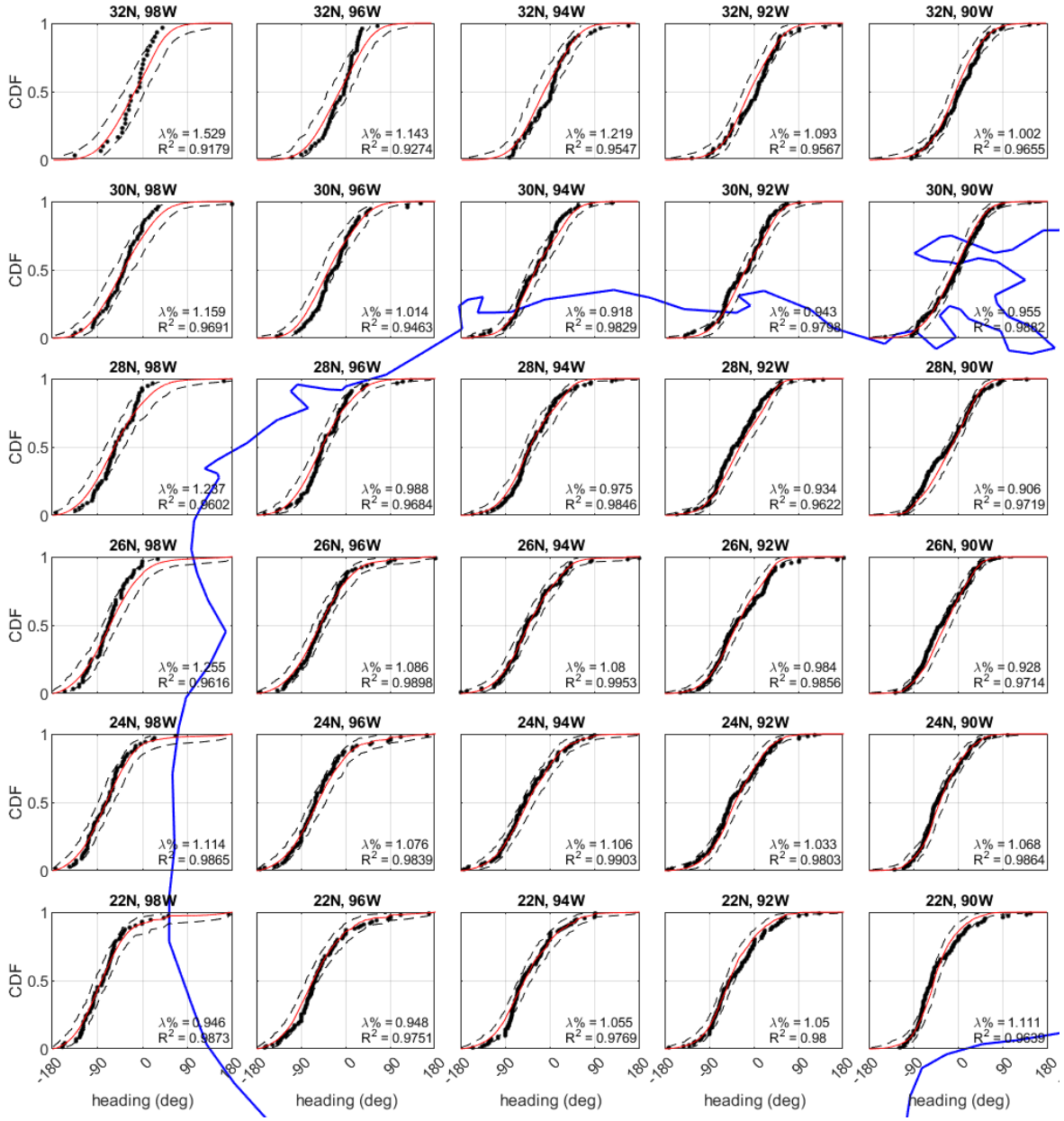

Figure 1. Comparison of the modeled (red line) and observed (black points) cumulative distribution functions (CDFs) for storm heading. Modeled and observed values are the heading of the storm at the time it was nearest to the center of a 250-km radius circle centered on the point indicated by the title of each graph. Observations are shown by black dots, modeled values are shown by red line, and 95% confidence bounds are shown by dashed black lines. Western Gulf of Mexico coastline is shown by blue line for orientation purposes.

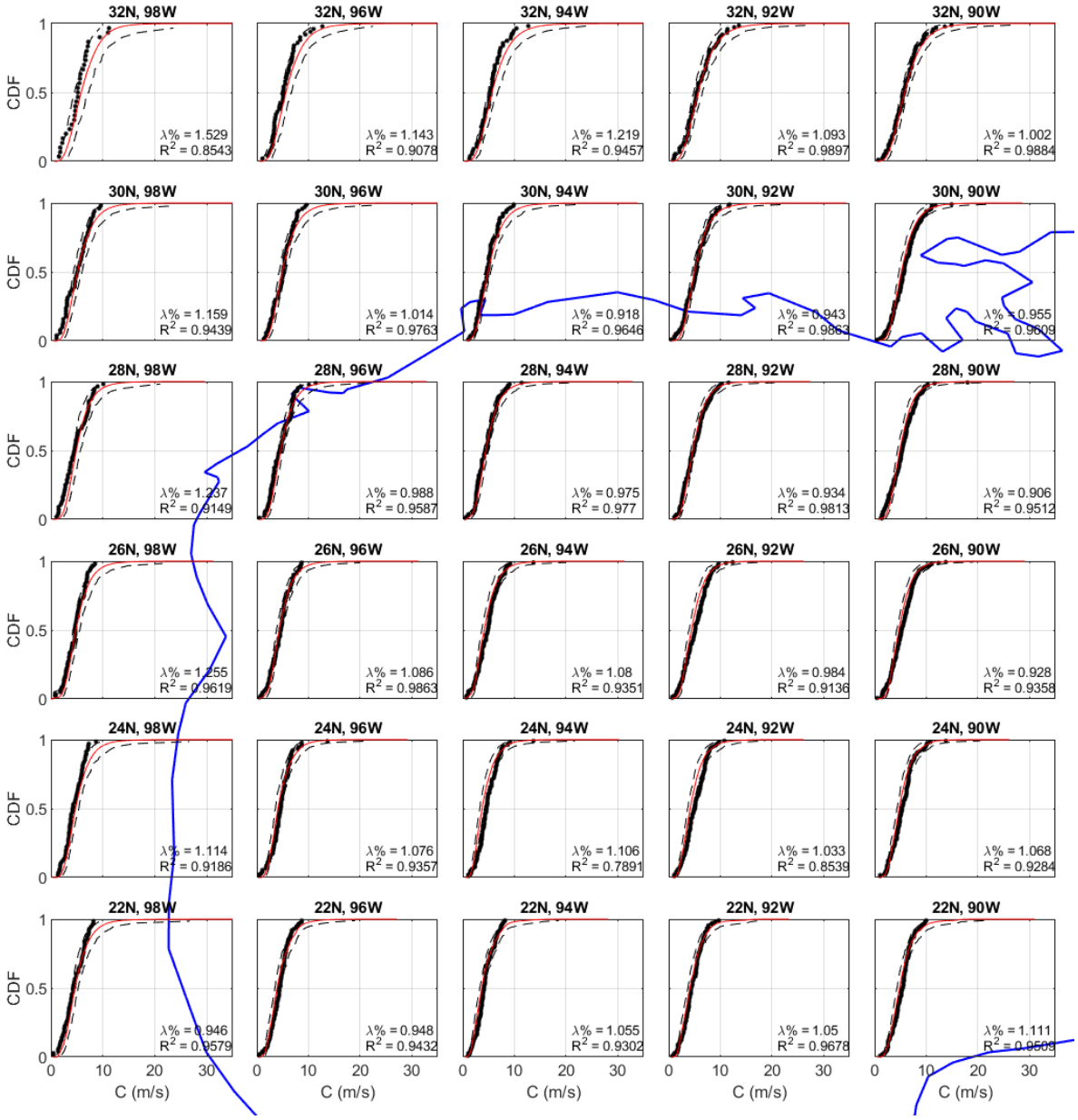

Figure 2. Comparison of the modeled (red line) and observed (black points) cumulative distribution function (CDF) for storm translation speed. Modeled and observed values are the storm translation speed at the time it was nearest to the center of a 250-km radius circle centered on the point indicated by the title of each graph. Observations are shown by black dots, modeled values are shown by red line, and 95% confidence bounds are shown by dashed black lines. Western Gulf of Mexico coastline is shown by blue line for orientation purposes.

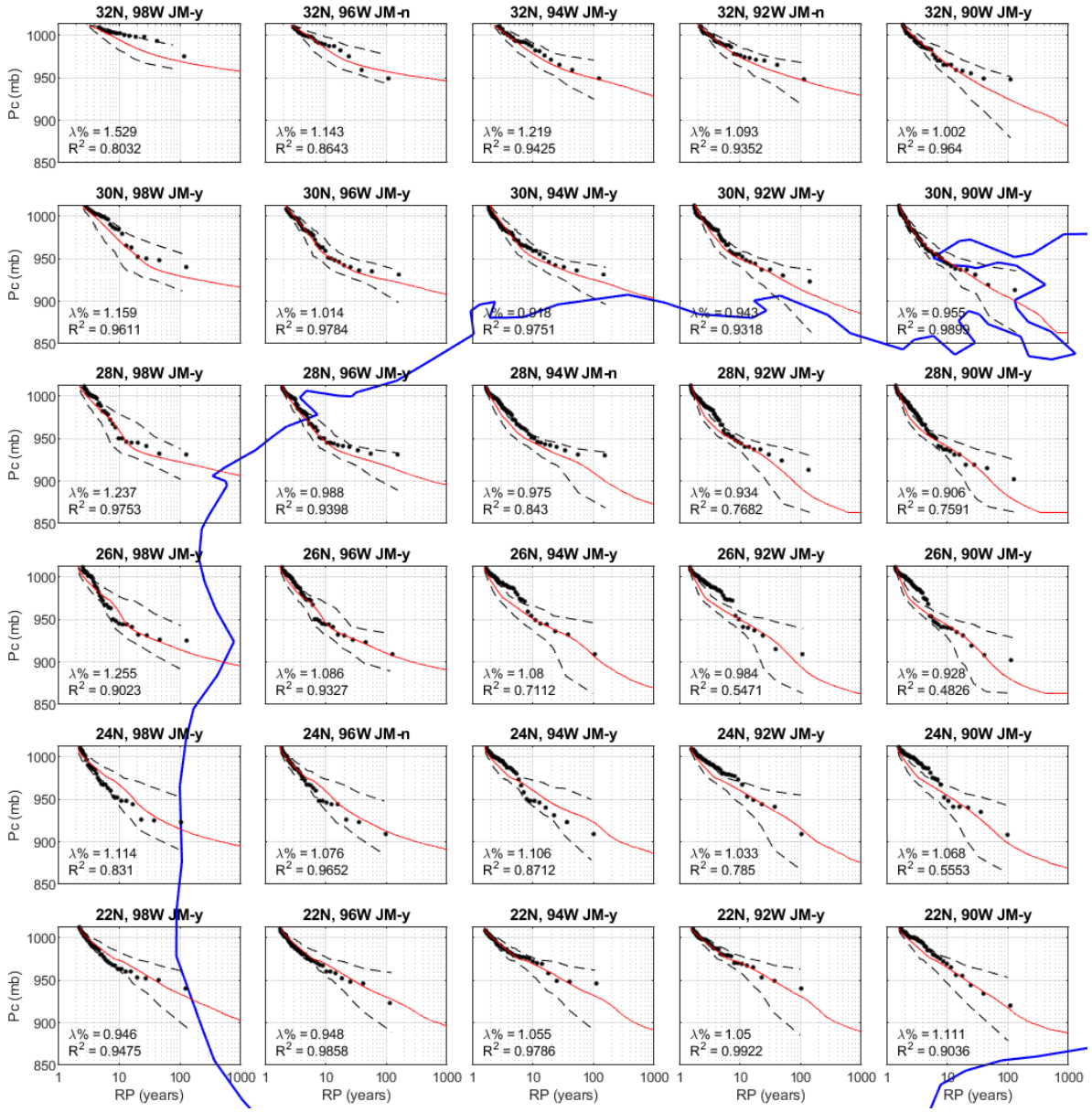

Figure 3. Comparison of modeled (red line) and observed (black points) central pressure plotted vs. return period. Modeled and observed values correspond to the minimum central pressure given in millibars (mb) while the storm is within a 250-km radius circle centered on the point indicated by the title of each graph. Observations are shown by black dots, modeled values are shown by red line, and 95% confidence bounds are shown by dashed black lines. Western Gulf of Mexico coastline is shown by blue line for orientation purposes. Note: JM-y indicates that the modeled central pressures pass the 95% confidence test using the James-Mason test.

In addition to the mean model estimates of pressure vs. return period in each of the plots given in Figure 3, these figures also present the 2.5th and 97.5th percentile (95% confidence range) values of central pressures derived by sampling Np different values of central pressure from the simulated storm set and computing the CDF and then the pressure return period (RP) curve using the model value of λ. This process was repeated 900 times, yielding 900 different RP curves based on sampling Np pressures randomly from the simulated storm set. The 900 different RP curves are then used to define the 95% confidence range for the mean pressure RP curves. In our testing, we include only tropical cyclones with central pressures less than 980 mbar, which is the threshold for a Category 1 event on the Saffir-Simpson hurricane scale. The pc-RP curves yield comparisons that include the combined effects of the modeling of central pressures and the frequency of occurrence of the storms.

Figure 4 presents a comparison of estimates of the landfall pressure as a function of return period. The historical data were obtained from HURDAT2 and Blake et al (2011). The Blake et al. (2011) data include central pressure information from all hurricanes that have made landfall in the United States. HURDAT2 was used to obtain information on the central pressures for all landfalling tropical storms. As in the case of the comparisons of central pressure plotted vs. return period developed from the data passing within 250 km of a given point, each of the plots given in Figure 4 also presents the 2.5th and 97.5th percentile (95% confidence range) values of central pressures derived by resampling. The historical data fall well within the range defined by the 95% confidence bounds.

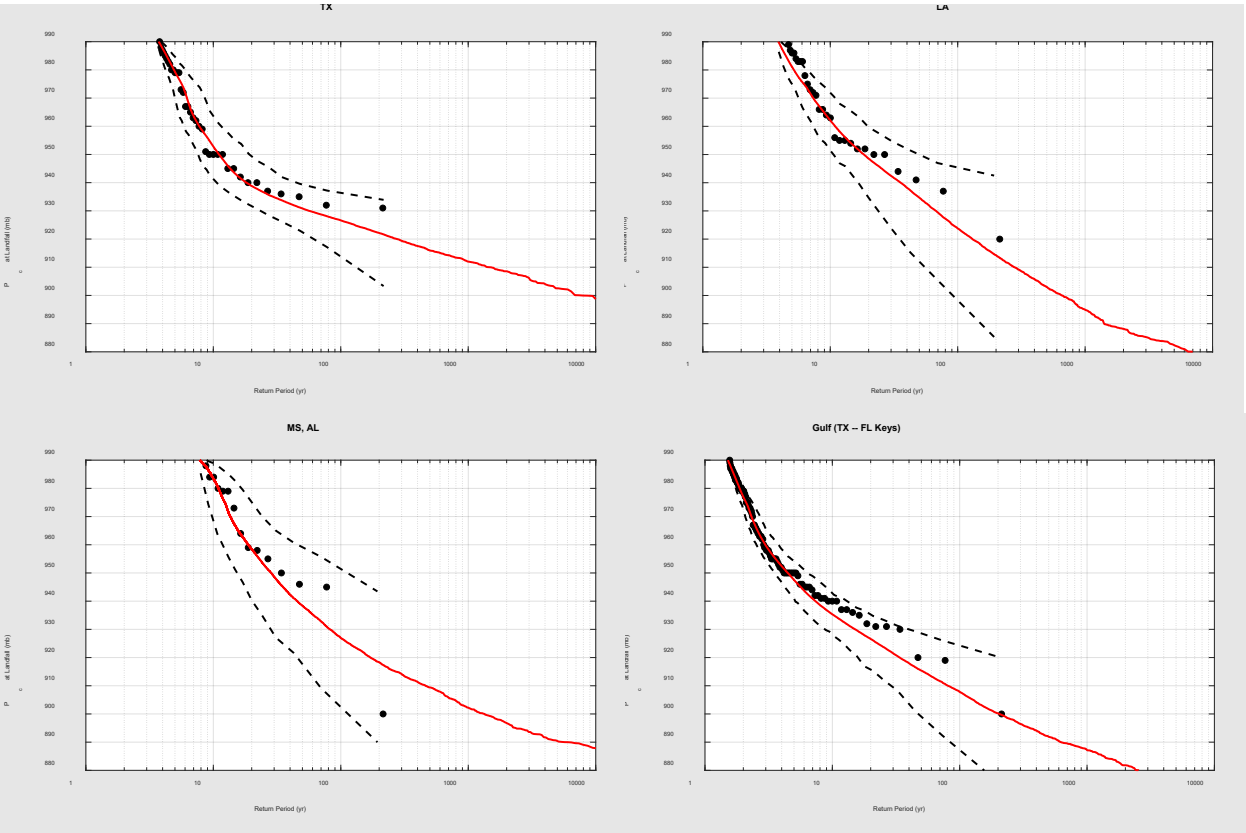

Figure 4. Comparison of modeled and observed central pressures at landfall along the Texas, Louisiana, Mississippi, and Alabama coastlines and the Gulf of Mexico coastline (Texas to Florida Keys). Observations are shown by black dots, modeled values are shown by red line, and 95% confidence bounds are shown by dashed black lines.

1.2 Hurricane Size and Pressure-Wind Modeling

The two key parameters controlling the extent of strong winds and the pressure-wind relationship are the *RMW*, which controls storm size, and the Holland *B* parameter, which describes the pressure-wind relationship used in the wind field model as well as the overall shape of the hurricane. In the synthetic hurricane model, statistical models for these two parameters have been developed. *B* and *RMW* are correlated with one another and with other hurricane parameters. The importance of the parameters and the development of the models are discussed in the following two sections.

1.2.1 Holland B Parameter Modeling

In some of the more modern hurricane risk models, a parameter commonly referred to as the Holland *B* parameter is used to define the pressure field and plays an important role in the risk prediction methodology (Vickery et al. 2000b, 2009; Powell et al. 2005).

Holland (1980) describes the radial distribution of surface pressure in a hurricane in the following form:

$$p(r) = p_c + \Delta p \cdot exp - \left[\frac{A}{r^B}\right] \tag{5}$$

where $p(r)$ is the surface pressure at a distance, *r*, from the storm center, p_c is the central pressure, Δp is the difference between the peripheral pressure and the central pressure, *A* is the location parameter, and *B* is the Holland pressure profile parameter. Holland (1980) showed that $RMW = A^{1/B}$ and thus Eq. 5 can be expressed as

$$p(r) = p_c + \Delta p \cdot exp - \left[\frac{RMW}{r}\right]^B \tag{6}$$

The gradient balance velocity, V_G, for a stationary storm is thus

$$V_G = \left[\left(\frac{RMW}{r}\right)^B \frac{B\Delta p \cdot exp\left[-\left(\frac{RMW}{r}\right)^B\right]}{\rho} + \left(\frac{rf}{2}\right)^2\right] - \frac{rf}{2} \tag{7}$$

where ρ is the density of air. The maximum wind speed at the *RMW* is

$$V_{Gmax} \approx \sqrt{\frac{B\Delta p}{\rho e}} \tag{8}$$

where *e* is the base of natural logarithms. In parametric hurricane wind field models where the input surface pressure field is defined by two parameters—Δp and a scale radius—the maximum wind speed in the simulated hurricane is proportional to $\sqrt{\Delta p}$. With the introduction of the additional term, *B*, the maximum wind speed in the simulated hurricane is proportional to $\sqrt{B\Delta p}$. The inclusion of *B* in Eq. 8 demonstrates how varying *B* changes the relationship between Δ*p*

and the maximum wind speed in a hurricane. Figure 5 presents example pressure profiles and gradient wind speed profiles associated with Eq. 5 through 7. When coupled with a simulation process, the additional term yields an increase in the variance of the output quantity (wind speed, wave height, and so on), resulting in a steeper hazard curve compared to models that do not include this additional term.

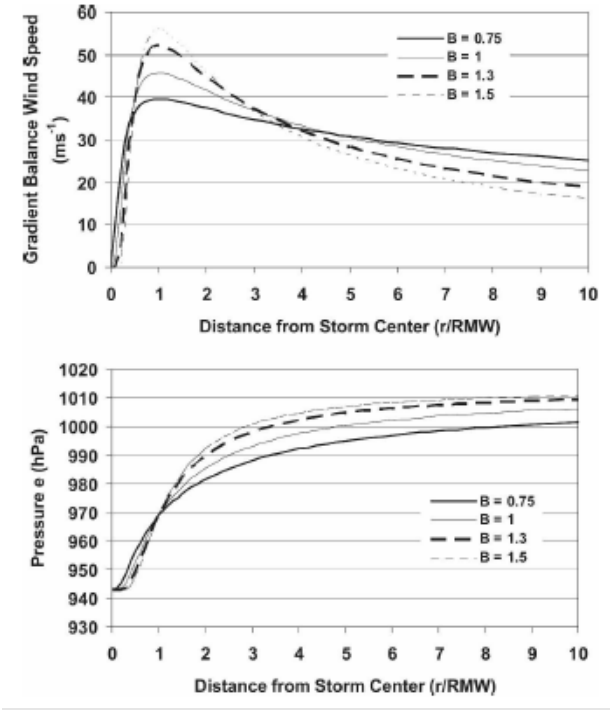

Figure 5. The effect of *B* on gradient-level wind speeds (top plot) and surface pressure (bottom plot) as a function of distance from the storm center.

hPa = hectopascal

From Vickery and Wadhera (2008), the value of B over open water is modeled as follows:

$$B = 1.76 - 1.21\sqrt{A} + \varepsilon;\ r^2{=}0.345,\ \sigma_B = 0.226 \tag{9}$$

where

$$A = \frac{RMW \cdot f}{\sqrt{2R_d T_s ln\left[1 + \frac{\Delta p}{p_c e}\right]}} \tag{10}$$

and ε is the random error term, sampled from a normal distribution with a mean of zero and standard deviation equal to σ_B.

In Eq. 10, RMW is the radius to maximum winds (m), f is the Coriolis parameter, R_d is the gas constant for dry air, T_s is the sea surface temperature in degrees C, p_c is the central pressure of the tropical cyclone, Δp (mb) is the difference between the p_c and the far field pressure (taken here as 1013 mb), and e is the base of natural logarithms.

The *A* term in Eq.10 is dominated by changes in latitude (through the Coriolis parameter) and *RMW*, with the net result being (from Eq. 9) that *B* decreases with both increasing latitude and increasing *RMW*. The increase in *RMW* and decrease in *B* result in storms that have a greater wave producing potential as they move north (for the same central pressure). The large storms produce larger waves than the smaller storms because of the increase in the fetch of high winds associated with the larger *RMW*.

1.2.2 Radius to Maximum Winds Modeling

In Vickery and Wadhera (2008), two models are given for the *RMW* in units of kilometers. One model is for Gulf of Mexico hurricanes and the other for Atlantic hurricanes. Here, the Atlantic storms *RMW* model is applied to Atlantic Basin hurricanes, and the Gulf of Mexico *RMW* model is applied to storms in the Gulf of Mexico. The models for *RMW* used in the simulation are

$$ln(RMW_{Atlantic}) = 3.015 - 6.291 \times 10^{-5}\Delta p^2 + 0.0337\Psi + \varepsilon_{Atlantic};\ r^2=0.297,\ \sigma_{\ln RMW} = 0.441 \quad (11a)$$

$$ln(RMW_{Gulf}) = 3.859 - 7.700 \times 10^{-5}\Delta p^2 + \varepsilon_{Gulf};\ r^2=0.290,\ \sigma_{\ln RMW} = 0.390 \quad (11b)$$

The two statistical models for the *RMW* (Gulf of Mexico and Atlantic Ocean) are combined to yield one *RMW* model for each simulated storm in the form

$$RMW = a_1 RMW_{Atlantic} + (1 - a_1)RMW_{Gulf} \quad (12a)$$

$$a_1 = \frac{\sum \Delta p_{Atlantic}}{\sum[\Delta p_{Atlantic} + \Delta p_{Gulf}]} \quad (12b)$$

where Δp is the central pressure difference and the summation is performed over all 6-hour time steps from storm origination to the current time. All simulated storm tracks containing the storm location (latitude and longitude), heading, central pressure, *RMW*, *B*, and translation speed are saved and later combined with the wind field model to compute wind speeds.

Equation 11a demonstrates that for Atlantic hurricanes, *RMW* decreases with increasing Δp and increases with increasing latitude. Recalling that *B* increases with decreasing *RMW*, we see that the more intense storms typical of the tropical latitudes tend to be tighter and yield higher wind speeds than the larger, more northerly, storms, even for the same central pressure.

1.3 Hurricane Wind Field Modeling

1.3.1 Hurricane Wind Field Model

The vortex model uses the results of the numerical solution of the two-dimensional, vertically integrated equations of motion of a translating hurricane. The asymmetries in a moving storm are a function of the translation speed of the storm and the nonlinear interactions between the wind velocity vectors and the frictional effects of the surface of the earth. The numerical solutions of the equations of motion of the hurricane have been solved separately for a storm translating over the ocean and for a storm translating over land. The separate solutions were developed because, in the over-water case, the magnitude of the surface drag coefficient is a function of the wind

speed itself, whereas in the over-land case, the magnitude of the surface drag coefficient is wind speed independent. The outputs of the numerical model represent the integrated boundary layer averaged wind speeds, representative of a long-duration average wind, taken as having an averaging time of 1 hour. The mean, 1-hour average, integrated wind speeds are then combined with a boundary layer model to produce estimates of wind speeds for any height and averaging time.

The variation of wind speed with height used in the hurricane model is described in Vickery et al. (2009a), and a summary is presented in Appendix A. The model used to describe the variation of the mean wind speed with height was developed using a combination of measured profiles derived from dropsonde data and a theoretical model described in Kepert (2001).

Turbulence near the surface is modeled as described in Vickery and Skerlj (2005) and is based primarily on the Engineering Sciences Data Unit (ESDU) methodology (ESDU 1982, 1983) models for the atmospheric boundary layer. The boundary layer model can deal with arbitrary terrain conditions (any surface roughness) changing both the properties of the mean flow field (i.e., the mean wind speed at a given height decreases with increasing surface roughness) as well as the gustiness of the wind (i.e., the gust factor increases with increasing surface roughness). The gust factor portion of the ESDU-based model has been validated through comparisons to gust factors derived from hurricane wind speed traces, as described in Vickery and Skerlj (2005).

1.3.2 Hurricane Wind Field Validation

The entire hurricane wind field model (overall flow field, boundary layer model, and gust factor model) has been validated through comparisons of simulated and observed wind speeds. These wind speed comparisons have been performed through comparisons of both the peak gust wind speeds and the average wind speeds. The comparisons show that the wind field model reproduces observed wind speeds well, matching both the gusts and the long period average winds. The model has been validated separately at offshore, coastal, and inland stations, considering the effects of local terrain and anemometer height on the measured and simulated wind speeds.

An example of the wind field validation is discussed in the following. The validation process includes validating not just the mean (or maximum gust) wind speeds but rather the validation process ensures that the model produces the correct time series of mean and gust wind speeds, wind directions, and surface pressures. Here, an example of the validation process shows that the model can simulate both marine- and land-based winds. The example storms are Hurricanes Bertha and Fran (1996), Hurricane Bonnie (1998), and Hurricane Ivan (2004). The tracks of the hurricanes and the locations of the measuring stations are given in Figure 6. Example comparisons of time series of mean and gust wind speeds, wind directions, and pressures are given in Figure 7. The comparisons clearly show that the model performs well in matching the observations of all parameters and their variation with time. Figure 8 presents summary scatter plots comparing the maximum values of the peak gust wind speeds from all stations on a storm-by-storm basis. The results show that the model is an unbiased estimator and performs equally well for marine- and land-based observations.

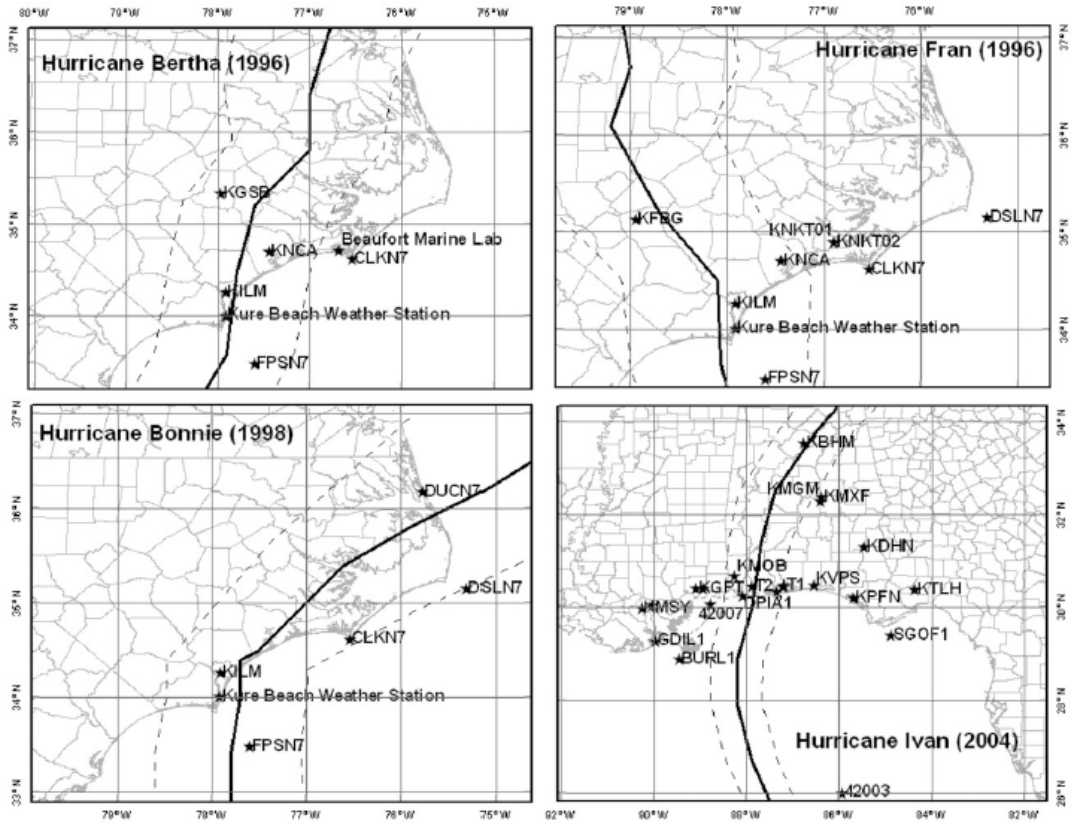

Figure 6. Tracks showing locations of marine- and land-based wind speed measurements. Dashed line represents the approximate distance of the radius to maximum winds.

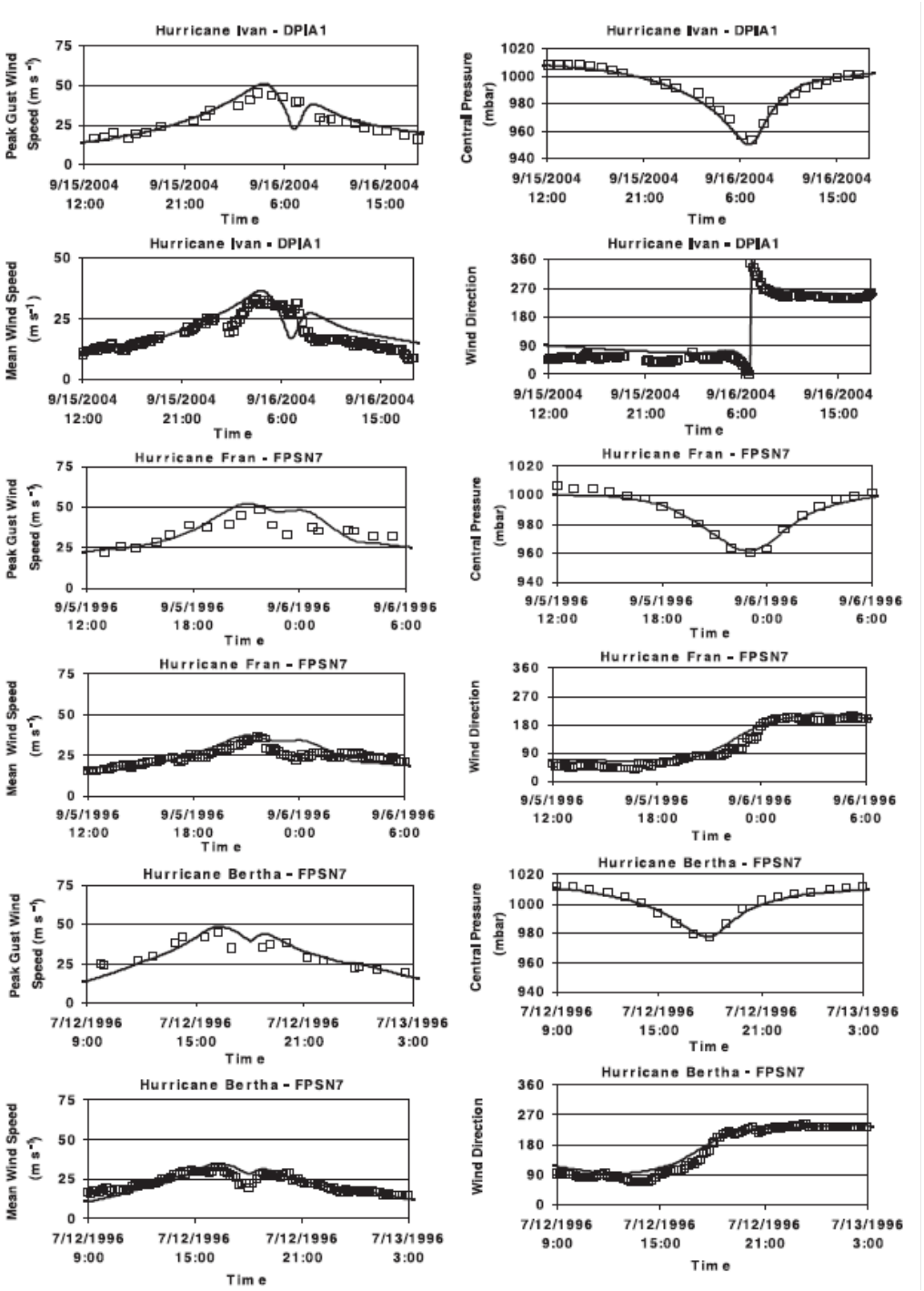

Figure 7. Example comparisons of modeled and observed gust and mean wind speeds, mean wind directions, and surface pressures at two Coastal-Marine Automated Network (C-MAN) stations from three hurricanes. In each of the three sets of plots, the upper left plot compares modeled and observed gust wind speeds (5-second running average values), the upper right plot compares modeled and observed surface pressures, the lower left plot compares modeled and observed mean wind speeds (data represent 10-minute means; model values represent hourly means), and the lower right plot presents wind directions.

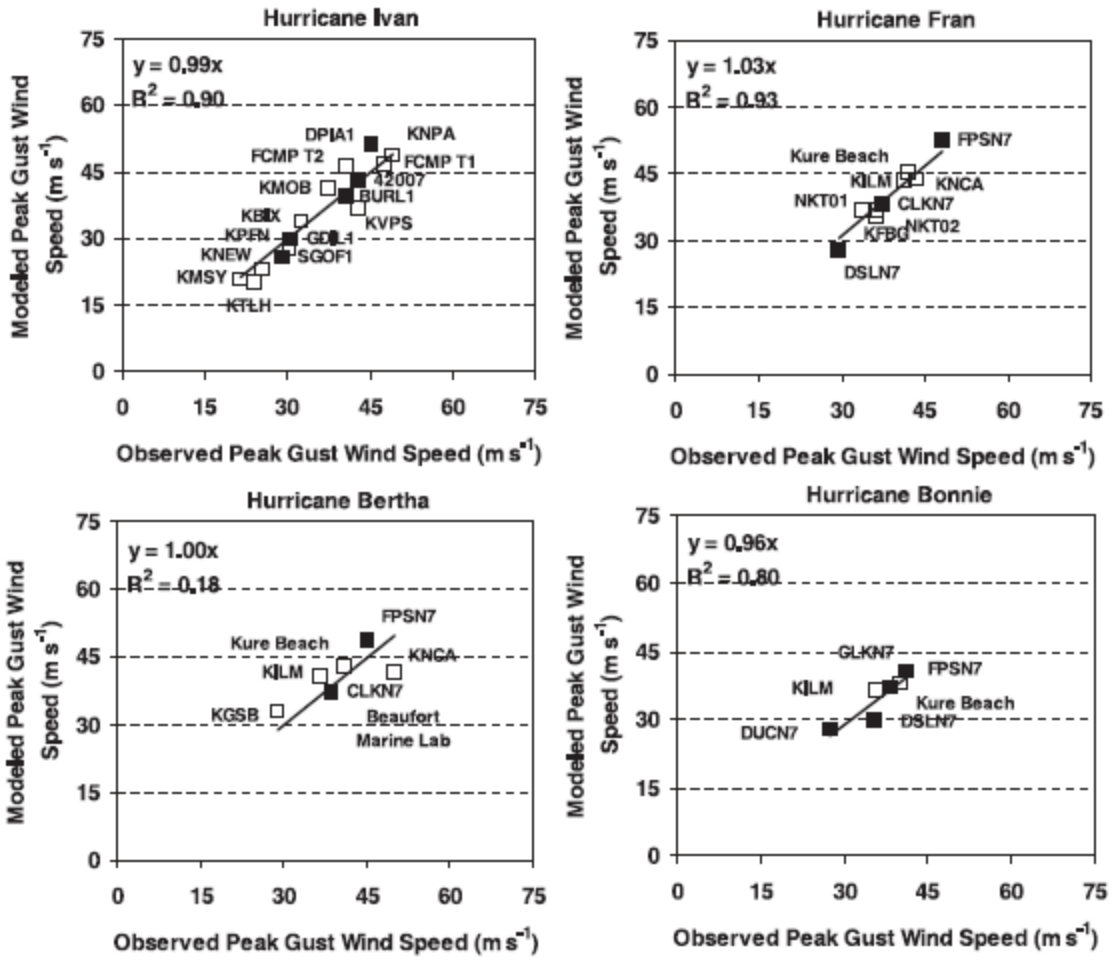

Figure 8. Comparisons of modeled and observed peak gust wind speeds for land-based and marine-based anemometers. Open squares represent land-based measurements, and solid squares represent marine-based measurements. All land-based wind speeds are representative of open terrain, and all marine-based measurements are representative of a marine terrain.

Figure 9 presents summary scatter plots of modeled and observed peak gust wind speeds for U.S. hurricanes making landfall between 1979 and 2005. The model comparisons indicate that the wind field mode is unbiased and performs well for a wide range of storm intensities, sizes, and geographic regions.

The hurricane wind field model used in this study is a physics-based model that has been extensively validated for both marine- and land-based stations. The model is coupled with a sea surface drag coefficient model that properly treats the limiting drag associated with high sea states. The variation of mean wind speed with height is based on dropsonde observations and properly models this variation. The ESDU-based gust factor model has been verified at heights ranging from 5 m above the sea surface (using buoy data) and up to 45 m above sea level (using C-MAN data).

The ability of the model to estimate surface-level mean winds, the variation of wind speed with height, and the near-surface turbulence characteristics (gust factors, turbulence intensities) of the hurricane allows the model to produce estimates of mean and gust wind speeds over a wide range of heights and is ideally suited for use in hazard studies for offshore facilities.

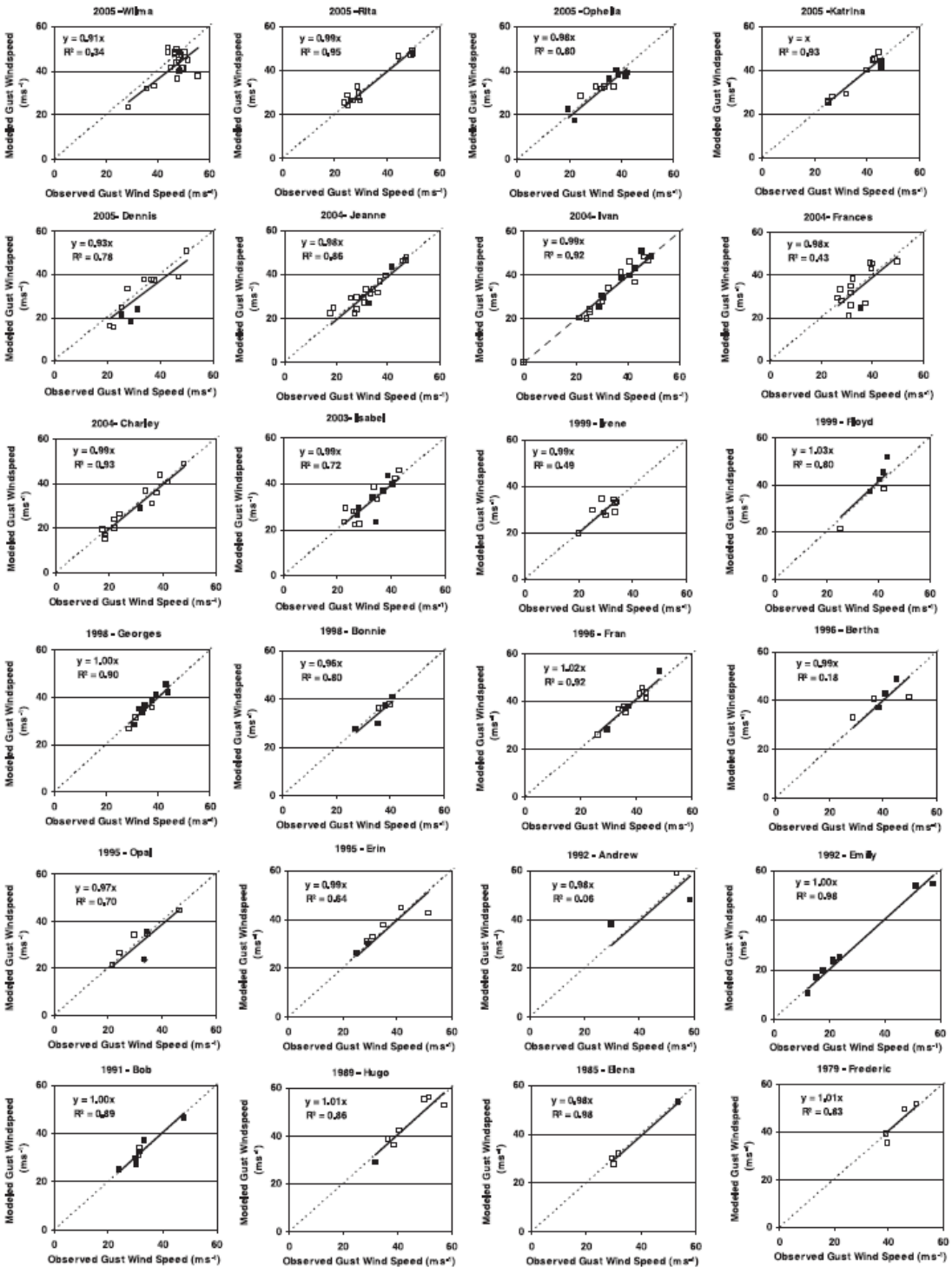

Figure 9. Comparisons of modeled and observed wind speeds from 24 landfalling hurricanes. Open squares represent land-based measurements, and solid squares represent marine-based measurements. All land-based wind speeds are representative of open terrain, and all marine-based measurements are representative of a marine terrain.

1.4 Analysis Methodology

Upon completion of a 500,000-year simulation, the wind speed data are rank ordered and then used to define the wind speed probability distribution, $P(v>V)$, conditional on a storm having passed within 250 km of the site. The probability that the tropical cyclone wind speed (independent of direction) is exceeded during time period t is

$$P_t(v > V) = 1 - \sum_{x=0}^{\infty} P(v < V|x)p_t(x) \tag{13}$$

where $P(v < V \mid x)$ is the probability that velocity v is less than V given that x storms occur, and $p_t(x)$ is the probability of x storms occurring during time period t. $P(v < V \mid x)$ is obtained by interpolating from the rank-ordered wind speed data. From Eq. 13, with $p_t(x)$ defined as Poisson and defining t as 1 year, the annual probability of exceeding a given wind speed is

$$P_a(v > V) = 1 - exp[-\lambda P(v > V)] \tag{14}$$

where λ represents the average annual number of storms approaching within 250 km of the site (i.e., the annual occurrence rate).

2 Harmonized Hurricane Terminology for Offshore Wind Design

Wind speeds specified in various design codes and those reported by the U.S. Weather Service are often associated with different averaging times. For example, the International Electrotechnical Commission (IEC) specifies a 10 minute average wind speed over an open water surface, whereas the U.S. wind loading standard—American Society of Civil Engineers (ASCE) 7—specifies a 3-s gust wind speed over open land and the U.S. Weather Service specifies a 1-min average wind speed, where in the case of a hurricane, the wind speed is usually associated with an open water terrain. In cases other than the IEC design standards, the specified wind speeds are at a height of 10 m. In the case of hurricanes, the conversion is wind speed dependent, and in all cases the conversion factors vary with height. Here, we present an approach for converting a wind speed specified with one averaging time to another averaging time to allow better comparisons between IEC wind turbine standards and the Saffir-Simpson hurricane categories.

The conversion of wind speed averaging times from one averaging time to another (e.g., from a 1-minute average to a 3-s gust) requires information on the turbulence characteristics of the hurricane boundary layer. The important turbulence characteristics relative to the effect of averaging time are the turbulence intensity and the velocity spectrum, which largely depend on the height of the boundary layer and the local surface roughness. The local surface roughness is a function of the mean wind speed and the surface drag coefficient. In addition to controlling the turbulence characteristics of the wind, the sea surface drag coefficient also controls the vertical shear, or rate of change of wind speed with height. The behavior of the surface drag coefficient as a function of wind speed and wave parameters has received significant attention since the study by Powell et al. (2003) was published. The Powell et al. (2003) paper showed that the drag coefficient appeared to reach a maximum value at mean wind speeds, at a height of 10 m, in the range of 20 to 30 meters per second (m/s) and then levels off or decrease as the wind speed increased. This observation conflicted with the general understanding that the sea surface drag coefficient increased monotonically with wind speed.

2.1 Sea Surface Drag Coefficient

Here we review many of the studies on the sea surface drag coefficient that have been published since 2003 to determine the model that best describes the behavior of the sea surface drag coefficient as a function of the mean wind speed. The sea surface drag coefficient in Powell et al. (2003) was developed by computing the variation of the mean wind speed with height over the lower 500 m of the hurricane boundary layer and then fitting the results of the lower 100 m to 200 m with a logarithmic boundary layer model, from which the aerodynamic surface roughness could be computed. The profiles were grouped into 10-m/s "bins," based on the mean wind speed averaged over the lowest 500 m. Wind speeds were obtained from Global Positioning System (GPS) dropsondes falling through the boundary layer. Details on the computation of wind speeds from the dropsondes are given in Hock and Franklin (1999). In addition to Powell et al. (2003), the dropsonde and mean velocity profile approach was used by Vickery et al. (2009a), Holthuijsen et al. (2012), Richter et al. (2016), and Ye et al. (2022). All these studies compute the sea surface drag coefficient using the flux-profile methodology outlined in the following.

Assuming a logarithmic profile, the variation of the mean wind speed with height, U(z), is given as

$$U(z) = \frac{u_*}{k} \ln\left(\frac{z}{z_0}\right) \tag{15}$$

Where u_* is the friction velocity, k is the von Karmen constant (k=0.4), z is height, and z_0 is the aerodynamic surface roughness. Eq. 15 can be rearranged to read

$$U(z) = \frac{u_*}{k} [\ln(z) - \ln(z_0)] \tag{16}$$

where it is readily seen that at $z = z_0$ is the height at which the mean wind speed theoretically equals zero. The surface shear stress, τ_0, is given as

$$\tau_0 = \rho u_*^2 = \rho C_{d_{10}} U^2(10) \tag{17}$$

where $C_{d_{10}}$ is the sea surface drag coefficient referenced to the mean wind speed at a height of 10 m above the local mean sea level. Combining Eq. 15 and 17 yields

$$C_{d_{10}} = \left[k / \ln\left(\frac{10}{z_0}\right)\right]^2 \tag{18}$$

Thus, given z_0, it is straightforward to compute $C_{d_{10}}$. Examples of profiles fitted to the logarithmic profile to estimate z_0 are shown in Figure 10. Figure 11 presents a summary plot of $C_{d_{10}}$ vs. $U(z)$ obtained from the data given in Powell et al. (2003), Vickery et al. (2009a), Holthuijsen (2012), Richter et al. (2016), and Ye et al. (2022).

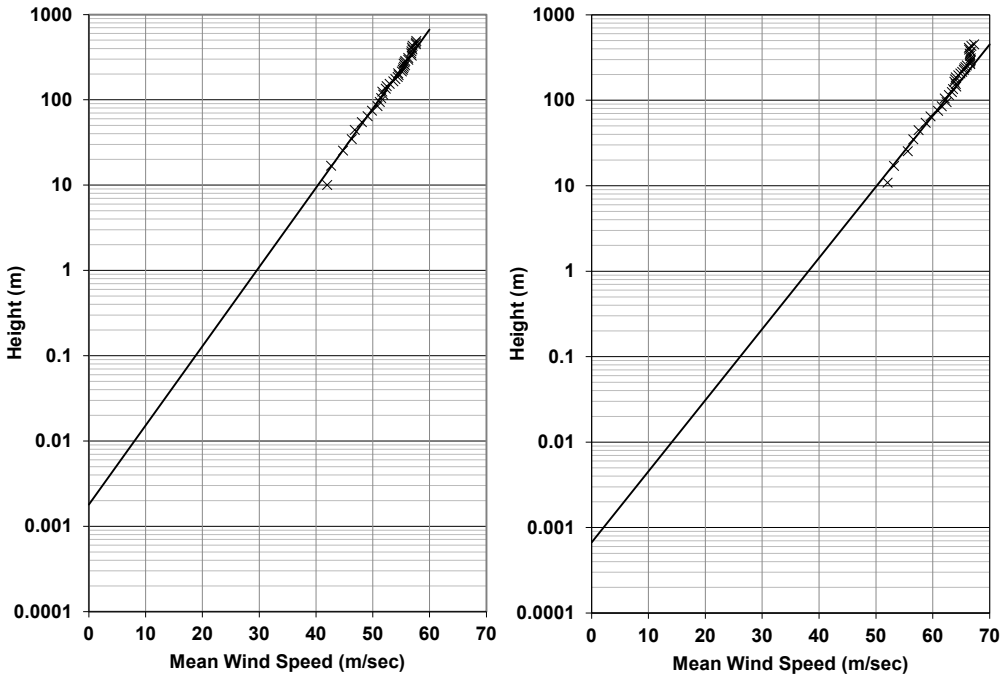

Figure 10. Example measured and fitted velocity profiles. Profiles fitted using method of least squares over a height range of 20 m to 150 m. Computed surface roughnesses in these examples are 0.0018 m and 0.00067 m for the left and right plots, respectively.

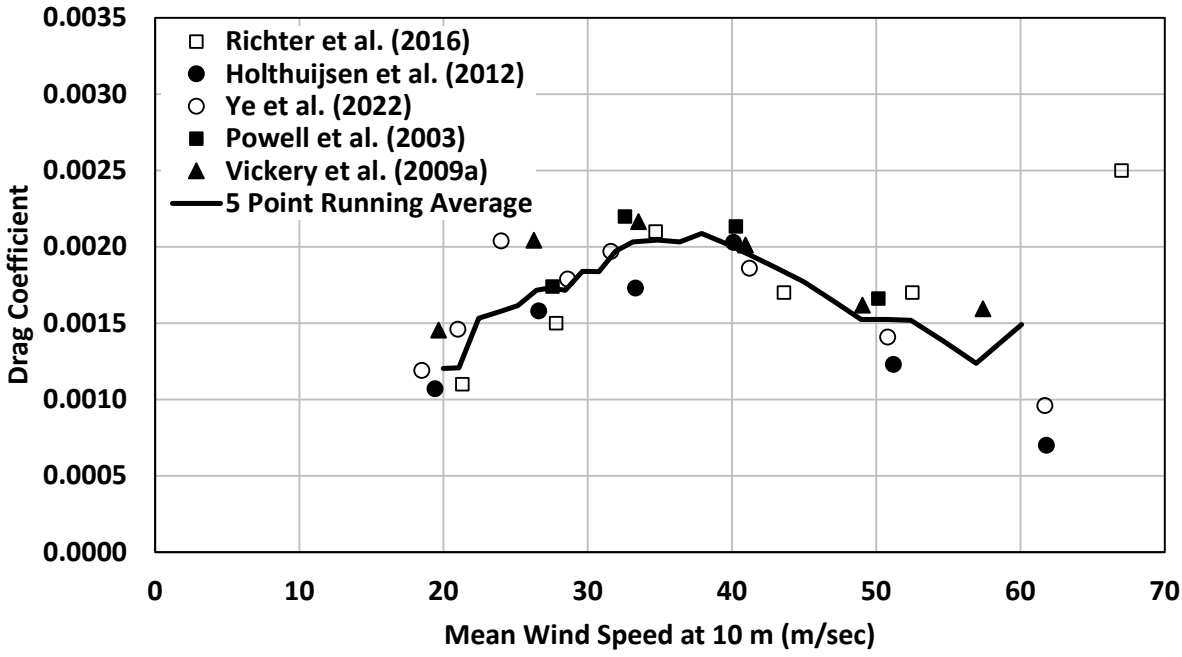

Figure 11. Variation of $C_{d_{10}}$ in tropical cyclones with mean wind speed from various studies obtained using the flux-profile method using GPS dropsondes

Gao et al. (2021), using an eddy-covariance method with data from aircraft flying through tropical cyclones, suggested that the sea surface drag coefficient reaches a maximum of 1.20×10^{-3} at a saturation wind speed of 33.5 m/s. However, the maximum wind speed in their dataset was only 28 m/s, and the saturation wind speed of 33.5 m/s was determined using the results of other studies. Vickers et al. (2013) also used aircraft eddy-covariance measurements to determine the relationship between $C_{d_{10}}$ and wind speed and found that $C_{d_{10}}$ reaches a maximum of about 2.3×10^{-3} at a mean wind speed of about 19 m/s. The data showed a decrease in $C_{d_{10}}$ as the wind speed increased beyond 19 m/s, but the maximum wind speed was only 23 m/s.

Laboratory studies performed by Takagaki et al. (2012) suggest that the drag coefficient reaches a maximum of about 2.58×10^{-3} for wind speeds greater than about 33 m/s. Donelan et al. (2004), also using laboratory studies, found that the drag coefficient reaches a maximum of about 2.5×10^{-3} at a wind speed of 33 m/s. Note that Curcic and Haus (2020) found an error in the computer code used in the Donelan et al. (2004) paper, which changed the saturation speed from 33 m/s to 29 m/s and increased the limiting value of $C_{d_{10}}$ from 2.5×10^{-3} to 3.0×10^{-3}. Troitskaya et al. (2012) also performed laboratory studies and found that the drag coefficient reaches a maximum of about 2.5×10^{-3} but at a mean wind speed at 10 m of about 50 m/s. Lee et al. (2022) suggest that laboratory experiments be used to determine $C_{d_{10}}$because the effects of wave age, fetch, wavelength, and sea spray are not modeled.

Donelan (2018) suggests that in addition to a wind speed dependence, $C_{d_{10}}$ is a function of the wind-sea Reynolds number, R_B, and wave age and that the reduction in drag coefficient above 30 m/s is largely associated with a wave sheltering effect, where a downstream trough is sheltered by flow separation at the crest of a wave—reducing the skin stress in the wave trough. The wind speed Reynolds number, R_B, is defined as

$$R_B = \frac{u_*^2}{\omega_p \upsilon} = \frac{T_s u_*^2}{2\pi\upsilon} \tag{19}$$

where υ is the kinematic viscosity of sea water and T_s is the significant wave period; wave age, β, is defined as

$$\beta = \frac{c_p}{U_{10}} \tag{20}$$

where c_p is the phase speed of the waves. In deep water, c_p is obtained from

$$c_p = \frac{g}{\omega} = \frac{gT_s}{2\pi} \tag{21}$$

Hsu et al. (2019) also suggest that $C_{d_{10}}$ is a function of the waves—they specifically suggest that $C_{d_{10}}$ is a function of the parameter ζ, defined as

$$\zeta = \frac{gT}{|U_{10}|cos\delta} = \frac{g\left(\frac{\chi}{U_h}\right)}{|U_{10}|cos\delta} \tag{22}$$

where g is the acceleration due to gravity, T is the duration the wind blows over a fetch of length χ, δ is the angle between $|U_{10}|$ and the surface waves, and U_h is the translation speed of the tropical cyclone.

Smith and Montgomery (2010, 2014) argue that the logarithmic law does not apply within the eyewall of a hurricane because the inward directed effective pressure gradient is largest at the surface where the tangential wind speed is at minimum and the magnitude of the radial (transverse) wind speed decreases with height in violation of the log law where the transverse wind speed increases with height. Consequently, the computation of an effective surface roughness using the approach used in Powell et al. (2003) and others is not valid. However, it could also be postulated that the use of the reduced drag coefficients at high wind speeds using a logarithmic profile near the surface produces the correct variation of the mean wind speed with height in or near the eyewall but for the wrong reasons.

Ye et al. (2022) also used the profile method to examine the behavior of $C_{d_{10}}$ at high wind speeds, focusing on the region near the radius to maximum winds. They found the same reduction in $C_{d_{10}}$ with wind speeds found in other studies using the profile method, but they postulated that the tropical cyclone dynamics play a role in affecting the validity of the profile method, e.g., as in Smith and Montgomery (2014). Richter et al. (2021) discuss the potential underestimate of $C_{d_{10}}$ at high wind speeds and, like Smith and Montgomery (2014), conclude that the flux-profile method may not be valid near the eyewall—suggesting that the flux-profile approach leads to an underestimate of the true value of $C_{d_{10}}$.

Some studies (e.g., Jaroz et al. 2007; Zou et al. 2018) have been performed to determine the behavior of $C_{d_{10}}$as a function of wind speed using estimates of the wind-induced currents in the ocean. Given information on the flow characteristics beneath the sea surface, the surface shear stress can be computed; given information on the mean wind speed at 10 m, $C_{d_{10}}$ can be obtained. In Zou et al. (2018), the wind speeds were estimated using the Holland et al. (2010) model for a hurricane wind field. Zou et al. (2018) did perform some wind field model validation, but the validation was performed where observed wind speeds were about 25 m/s but at the locations where the ocean current information was obtained experienced modeled wind speeds of about 50 m/s. Jaroz et al. (2007) did not indicate how they arrived at the wind speeds needed to compute $C_{d_{10}}$. Consequently, drag coefficients from these studies were not used in subsequent analyses presented herein.

Peng and Lee (2015) used storm surge model validation studies to confirm the existence of a decreasing $C_{d_{10}}$ at high wind speeds. Peng and Lee (2015) modeled the wind field using the Holland (1980) representation of the hurricane wind field, but no validation of the model was performed for any of the storms for which the storm surge was modeled. Considering the likely large errors associated with the wind field model as well as errors introduced by the storm surge model itself, the results of this study are questionable.

The reduction in $C_{d_{10}}$ has also been postulated to be a result of sea spray. This was suggested in Powell et al. (2003), but others have since addressed the issue using models for momentum transfer related to the formation of spray and its injection into the wind and subsequent falling back into the water. Andreas (2004) argues that $C_{d_{10}}$, including the effects of sea spray, can be modeled using

$$C_{d_{10}} = \left[1 - 6.5 \times 10^{-5} \left(\frac{\rho_w}{\rho_a}\right) u_*^2\right] \left[k / \ln\left(\frac{10}{z_0}\right)\right]^2 \quad (23)$$

where ρ_w and ρ_a are the densities of sea water and air, respectively. Andreas (2004) points out that the use of Eq. 23 is suggestive rather than conclusive but demonstrates that the spray term serves to reduce the sea surface drag coefficient. Makin (2005) develops a model for $C_{d_{10}}$ incorporating sea spray and the critical wind speed (33 m/s) implied in Powell et al. (2003). In incorporating sea spray, Makin (2005) in their model for $C_{d_{10}}$ also includes some wave parameters but by ignoring fetch they can relate the wave parameters to U_{10}. Makin proposes a two-layer model with a thin inner sea surface suspension layer and a logarithmic boundary layer above the suspension layer. Makin postulates that the height of the suspension layer is greater than the height of the short breaking waves, which are much less than the significant wave height.

Liu et al. (2012) also developed a model for the sea surface drag coefficient as a function of wind speed and wave age by extending the work of Makin (2005). For large β, the shape of the Liu et al. (2012) model produces a reasonable match of the $C_{d_{10}}$ versus U_{10} characteristics given Powell et al. (2003). However, both Makin (2005) and Liu et al. (2012) use the fact that $C_{d_{10}}$ in Powell et al. (2003) reaches a maximum for U_{10} equal to 33 m/s and then postulated that the effect of sea spray on $C_{d_{10}}$ could be ignored for wind speeds less than 33 m/s.

Shi et al. (2016), using the two-layer approach, developed a model for the total drag coefficient including the effects of sea spray. The model relates sea spray to R_B and because wave age is needed to compute T_s for the computation of R_B, the shape of the resulting $C_{d_{10}}$ versus U_{10} is different for each wave age examined. The higher the wave age, the lower the magnitude of U_{10} at which $C_{d_{10}}$ reaches a maximum. In the case of a fully developed sea, β=1.2, Shi et al. (2016) indicate that $C_{d_{10}}$ reaches a maximum of about 2.5×10^{-3} at U_{10}~25 m/s and, for fully developed waves, the estimated value of $C_{d_{10}}$ becomes zero for U_{10} = 40 m/s. It is worth noting that waves in hurricanes are not fully developed.

Vickery et al. (2009a) present the only $C_{d_{10}}$data determined using the flux method that are outside the RMW. These data do not show $C_{d_{10}}$reaching a maximum at a wind speed of about 33 m/s but rather show a slow increase in $C_{d_{10}}$ with wind speed beyond the 33 m/s threshold. The highest 10-m wind speed for the outside RMW case was about 45 m/s. Considering that outside RMW no decrease in $C_{d_{10}}$ is seen suggests that Smith and Montgomery's (2014) suggestion that the log law does not apply near RMW and the flux method underestimates $C_{d_{10}}$ may be correct. If this is the case, the use of a drag coefficient wind speed relationship such as given in Figure 12 will produce good estimates of the variation of the mean wind speed with height, but it would

understate the turbulence in the hurricane boundary layer because of a potential underestimate of the true value of $C_{d_{10}}$.

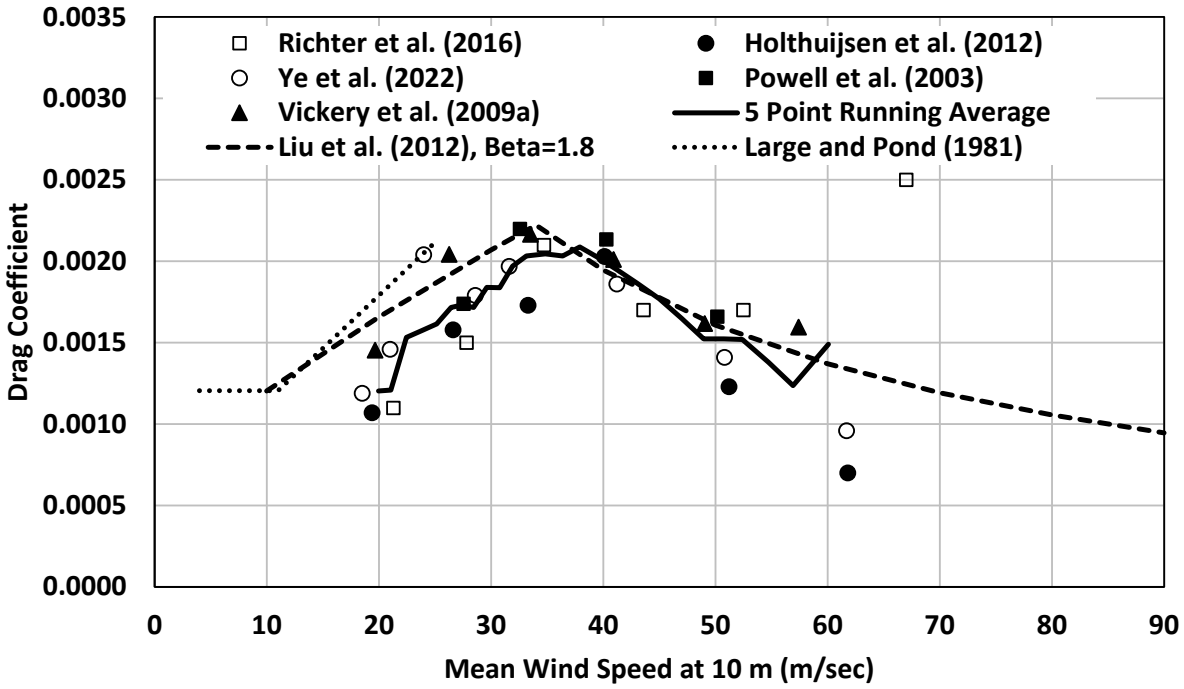

Figure 12. Variation of $C_{d_{10}}$ in tropical cyclones with mean wind speed from various studies obtained using the flux-profile method using GPS dropsondes plus the model given in Liu et al. (2012) and the Large and Pond (1981) model for wind speeds less than 25 m/s

2.2 Gust Factors

The characteristics of the near-surface turbulence within the marine boundary layer are needed to estimate peak wind speeds, turbulence intensities, velocity spectra, and so on. Unfortunately, there are very few detailed measurements of turbulence in hurricanes over the ocean. There are time series of wind speeds from offshore platforms, but these data are proprietary. High-resolution wind speed traces are not stored by the National Oceanic and Atmospheric Administration (NOAA)/National Climatic Data Center, whose data are limited to mean wind speeds (of various durations) and peak gust wind speeds (of various averaging times). Thus, the structure of the atmospheric turbulence is limited to the analysis of the gust factors. Unfortunately, direct passages of the eyewall over a NOAA data buoy or C-MAN station, without failures of the anemometry, are rare. To date, the highest 10-minute mean wind speed at a NOAA station is 56.4 m/s, which was recorded at C-MAN station FYWF1 during Hurricane Andrew in 1992, but this was at a height of 43.9 m, and higher winds likely occurred afterwards.

2.2.1 Gust Factor Data From He et al. (2020)

He et al. (2020) report marine gust factors for mean wind speeds greater than 70 m/s, but these data were recorded during Super Typhoon Hato using wind speed data recorded with an anemometer mounted on a 6.5-m mast, located at an elevation of 60 m above sea level on the

small island of Huangmaozhou, in the South China Sea. The typhoon passed almost directly over the anemometer which experienced high winds approaching first from the northwest and second from the southeast. The location of the anemometer on the island and the approximate range of wind directions associated with each passage of the high winds are shown in Figure 13.

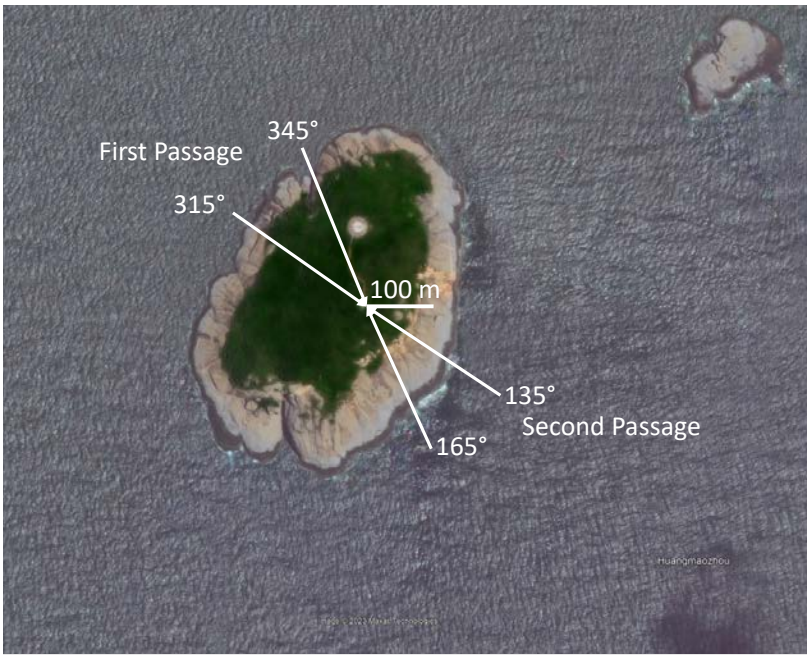

Figure 13. Image of the small island Huangmaozhou showing the location of the anemometer and the wind directions associated with the first and second passages of high winds. In the first passage, the anemometer is located about 200 m from the shoreline; for the second passage, the anemometer is about 150 m from the shoreline.

The anemometer recorded the maximum 3-s gust speed and average 1-min wind speed every minute. He et al. (2020) used these data to compute the 3-s gust factor defined as the maximum 3-s gust wind speed each minute divided by the 1-min mean wind speed in each interval. These gust factor data were averaged and binned into 10-m/s bins. A summary of the gust factors from He et al. (2022) is presented in Table 1, where the mean and standard deviation of the gust factor are provided as well as the number of samples.

The mean gust factors in each bin are plotted versus wind speed in Figure 14. Because the wind speeds were averaged within each bin, the wind speeds represent a long-term mean void of turbulence (e.g., 10 minutes to an hour) rather than individual 1-min means; thus, the horizontal axis represents a mean wind speed rather than a 1-min wind speed—but a precise estimate of the effective averaging time is difficult to ascertain because the 1-min wind speeds and associated gust factors were sorted before being averaged. Also shown in Figure 14 are the 1-min gust factors computed using the ESDU (1982, 1983) formulations for the gust factor coupled with the sea surface drag coefficient computed using three different assumptions. The sea surface drag coefficient models include that proposed by Large and Pond (1981) with maximum values of 0.0019 and 0.0023 and the model of Liu et al. (2012) computed using a β of 1.8. The maximum values of 0.0019 and 0.0023 are approximately the lower and upper bounds of the radius-

dependent model used for $C_{d_{10}}$ discussed in Vickery at al. (2009a) and implemented in the hurricane model used to develop the wind hazard data presented herein. The upper bound is a bit lower than that used in Vickery et al (2009a) but is consistent with the data presented in Figure 11.

Table 1. Gust Factor Data From He et al. (2020)

Wind Speed at 66.5 m (m/s)	First Passage			Second Passage		
	N[1]	G(3,60)[2]	Std. Dev.	N[1]	G(3,60)[2]	Std. Dev.
10–15	93	1.16	0.04	62	1.14	0.04
15–20	167	1.17	0.05	82	1.15	0.04
20–30	140	1.20	0.05	73	1.19	0.05
30–40	19	1.28	0.08	32	1.18	0.05
40–50	7	1.33	0.07	32	1.20	0.06
50–60	13	1.26	0.06	6	1.18	0.05
60–70	1	1.17		17	1.15	0.03
70–75				6	1.13	0.03

[1] N = Number of samples

[2] G(3,60) = 3-s peak gust wind speed recorded over a 60-s period divided by the mean wind speed averaged over 60 seconds

The modeled gust factors were computed assuming that the average wind speeds given in Table 1 are representative of a 10-min mean winds speed (i.e., maximum 10-min mean within an hour). The gust factors associated with the first and second passages yield similar trends of the gust factor, first increasing with wind speed, reaching a maximum and then decreasing; however, the maximum gust factors from the first and second passages are notably different: The gust factors from the first passage are much higher than those from the second passage for wind speeds between 30 m/s and 50 m/s.

It is not clear how the mean and gust wind speeds may have been influenced by the effects of the local terrain and topographic speed-ups induced by the island's terrain and topography. However, for each passage of strong winds, the influence of terrain, fetch, and wind speed-ups would not be expected to vary significantly because the range of directions associated with the strong winds is relatively narrow. The maximum wind speed of 72 m/s at a height of 66.5 m above sea level (ASL; shown in Figure 14) corresponds to a maximum average wind speed at a height of 10 m of about 61 m/s.

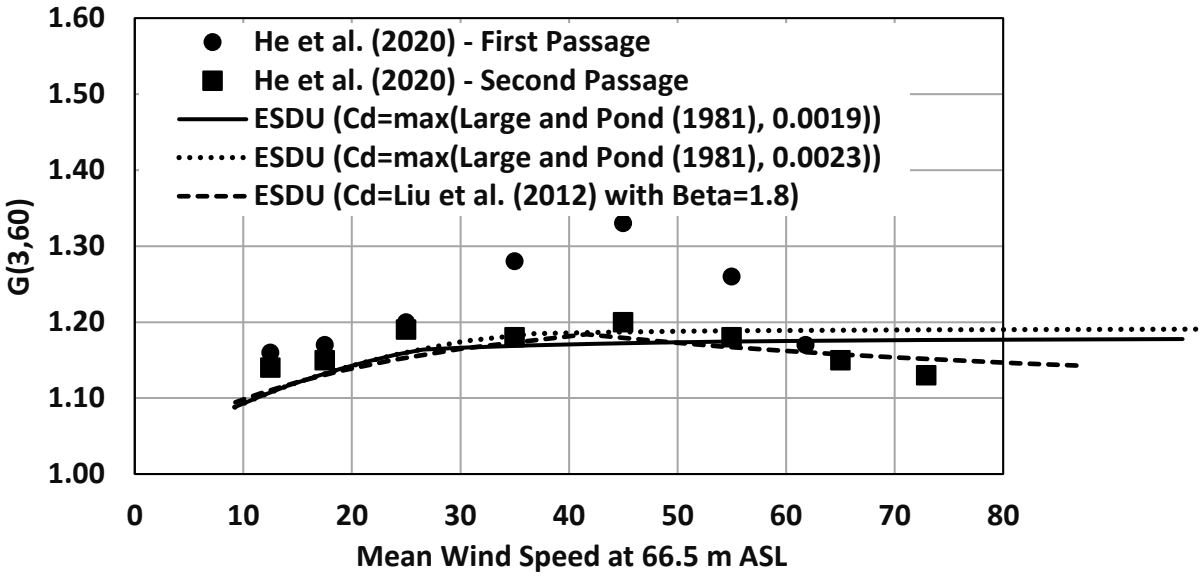

Figure 14. Modeled and measured (He et al. 2020) gust factors in high winds in the South China Sea

Statistics of the differences and the R^2 values associated with the comparison of the three gust factor models to the gust factor data from the second passage shown in Figure 14 are summarized in Table 2. Not surprisingly, the model of Liu et al. (2012), as implemented here, produces the highest R^2, with the R^2 values from both Large and Pond (1981) models being negative.

Table 2. Quantitative Comparisons of Model and Observed Gust Factors, G(3,60) at a Height of 66.5 m. Observed Gust Factors From Passage Two as Given in He et al. (2020).

Data (He et al. 2022)		C_d (L&P, 0.0019)		C_d (L&P, 0.0023)		C_d (Liu et al. 2012)	
U(66.5,600)[1]	G(3,60)[2]	G(3,60)[2]	Error	G(3,60)[2]	Error	G(3,60)[2]	Error
12.5	1.14	1.11	-0.033	1.11	-0.033	1.11	-0.031
17.5	1.15	1.13	-0.019	1.13	-0.019	1.13	-0.020
25.0	1.19	1.16	-0.032	1.16	-0.032	1.15	-0.038
35.0	1.18	1.17	-0.012	1.18	0.004	1.17	-0.008
45.0	1.20	1.17	-0.028	1.19	-0.013	1.18	-0.019
55.0	1.18	1.17	-0.006	1.19	0.008	1.17	-0.011
65.0	1.15	1.18	0.026	1.19	0.039	1.16	0.009
72.9	1.13	1.18	0.046	1.19	0.060	1.15	0.023
Mean	1.165	1.158	-0.007	1.167	0.002	1.153	-0.012
Std. Dev.	0.026	0.026	0.029	0.032	0.034	0.024	0.020
R^2			-0.264		-0.708		0.377

[1] U(66.5,600) = Mean wind speed at a height of 66.5 m averaged over a period of 600 seconds

[2] G(3,60) = 3-s peak gust wind speed recorded over a 60-s period divided by the mean wind speed averaged over 60 seconds

Note: L&P = Large and Pond (1981)

2.2.2 Gust Factor Data From NOAA Stations

All C-MAN data were collected from hurricanes affecting the Atlantic coast, and all buoy data were from Gulf of Mexico hurricanes. Both C-MANs and buoys report the maximum 5-s gust occurring in a 1-hour period, the time at which the gust occurred, and a 10-min mean wind speed every 10 minutes. In the case of the buoy data, only data from the 10-m buoys were considered because wind data from buoys with anemometer heights of 3 m and 5 m are thought to have been influenced by the local sea state because they drop into the wave troughs where sheltering is expected.

A difficulty encountered when comparing the measured gust factors to modeled gust factors is associated with the lack of stationarity[1] within the hurricane wind speeds and the fact that there is only one measurement of the gust wind speed during the hour, but there are six 10-min means recorded during the 1-hour period—hence, five other gust factors that may have (but not necessarily) all been lower than the one computed gust factor, which used the largest gust wind speed within the hour.

Here, the measured gust factors are defined using two methods:

[1] A stationary process has the property that the mean, variance, and other statistics do not change over time.

- The largest gust recorded during a 1-hour period divided by the 10-min mean wind speed recorded during the time at which the gust was measured
- The largest gust recorded during a 1-hour period divided by the 30-min mean wind speed computed using the average of the 10-min wind speed recorded during the time at which the gust was measured and the 10-min wind speeds occurring immediately before and after the 10-min mean winds speed recorded during the time at which the gust was measured.

C-MAN Gust Factors. The anemometer heights for C-MANs DSLN7, FPSN7, and FWYF1 are 46.6 m, 44.2 m, and 43.9 m, respectively. All gust factor data from these three C-MANs were combined, with the analytic estimates of the gust factor using the average height of 44.9 m. Summaries of the gust factors from the C-MAN stations are presented in Table 3 and Table 4, where the mean and standard deviation of the gust factor are provided as well as the number of samples in each wind speed bin. There are only ten 10-min mean wind speeds greater than 40 m/s and only eight 30-min mean wind speeds greater than 40 m/s.

The difference in the estimates of the gust factor computed using the 10-min or 30-min mean wind speeds is negligible, with a maximum difference of less than 1% and an average difference of less than 0.1%, suggesting that the use of the 10-min mean wind speed within which the hourly peak gust wind speed was recorded is representative of G(5,3600).

Figure 15 and Figure 17 present gust factors computed from wind speed data obtained from the C-MAN stations during hurricanes along with the gust factors computed using the capped Large and Pond (1981) representation of the drag coefficient as well as the drag coefficient described in Liu et al. (2012). There are only ten 10-min mean wind speeds greater than 40 m/s and only eight 30-min mean wind speeds greater than 40 m/s.

Table 3. Five-S Gust Factors From C-MAN Stations DSLN7, FPSN7, and FWYF1. Measured Gust Factors Computed Using a 10-Min Mean Wind Speed.

U(44.9,600)[(1)] (m/s)	G(5,3600)[(2)]	Std. Dev. (m/s)	N[(3)]
12.4	1.24	0.125	249
17.2	1.25	0.094	157
22.4	1.26	0.084	137
27.1	1.31	0.093	78
32.4	1.28	0.091	50
36.8	1.30	0.102	17
43.1	1.25	0.077	8
48.5	1.36		1
56.4	1.34		1

(1) U(44.9,600) = Mean wind speed at a height of 44.9 m averaged over a period of 600 seconds

(2) G(3,3600) = Maximum 5-s peak gust recorded during a 3,600-s period divided by the mean wind speed averaged over 600 seconds

(3) N = Number of samples

Table 4. Five-S Gust Factors From C-MAN Stations DSLN7, FPSN7, and FWYF1. Measured Gust Factors Computed Using a 30-Min Mean Wind Speed.

U(44.9,1800) (m/s)	G(5,3600)	Std. Dev. (m/s)	N
12.4	1.24	0.138	250
17.2	1.24	0.094	156
22.2	1.26	0.079	130
27.0	1.31	0.098	86
32.3	1.27	0.094	49
36.4	1.31	0.095	19
42.3	1.25	0.071	7
48.6	1.36		1

(1) U(44.9,600) = Mean wind speed at a height of 44.9 m averaged over a period of 600 seconds

(2) G(5,3600) = Maximum 5-s peak gust recorded during a 3,600-s period divided by the mean wind speed averaged over 1,800 seconds

(3) N = Number of samples

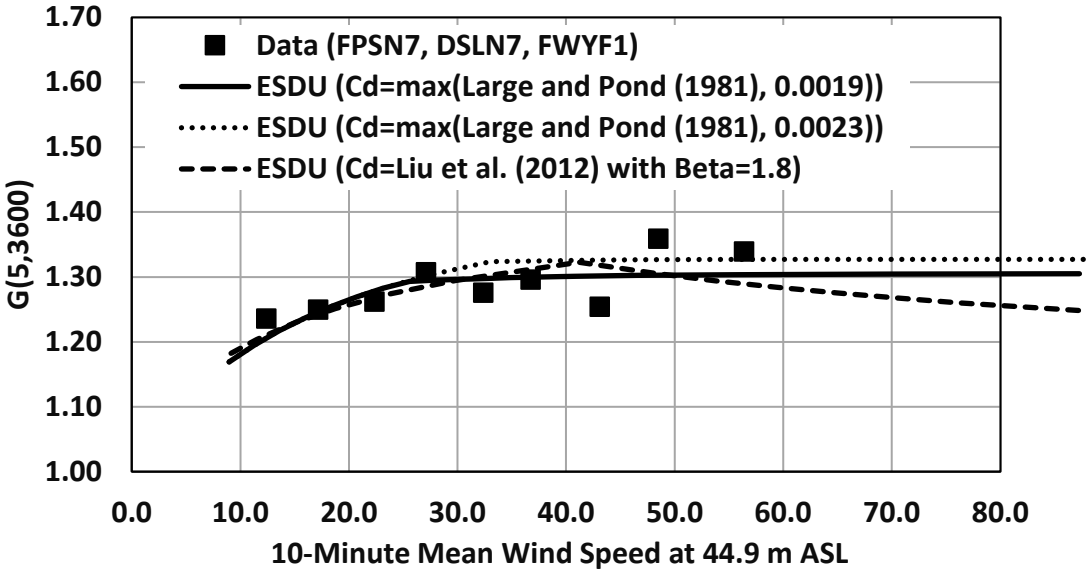

Figure 15. Modeled and measured gust factors at a height of 44.9 m. Measured gust factors from NOAA C-MAN stations based on a 10-min mean wind speed.

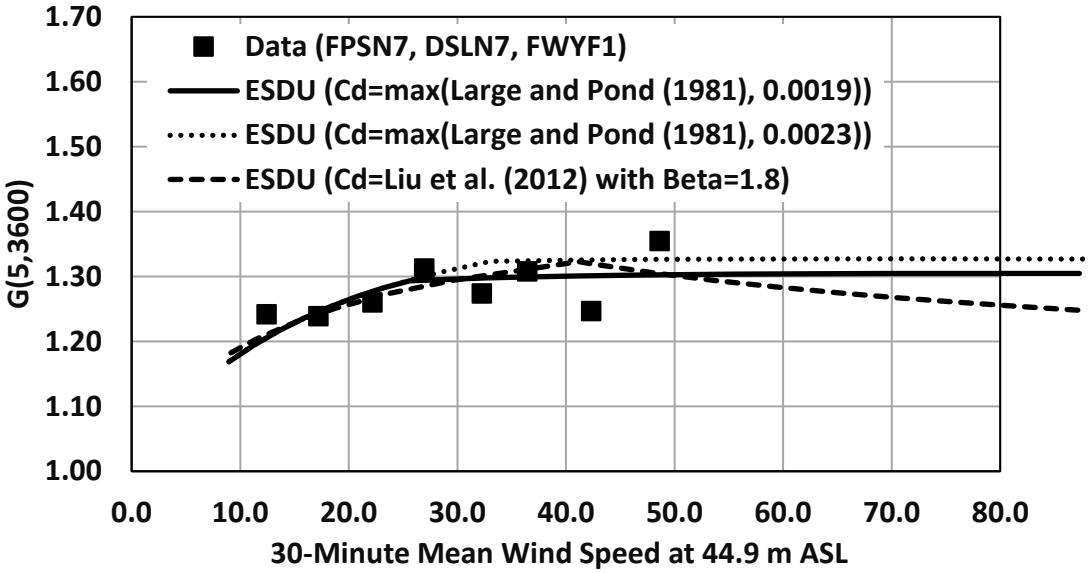

Figure 16. Modeled and measured gust factors at a height of 44.9 m. Measured gust factors from NOAA C-MAN stations based on a 30-min mean wind speed.

Tables 5 and 6 present the data presented in Figures 15 and 16, respectively, along with the error (difference between the modeled and observed gust factors) for the three different modeled representations of the sea-surface drag coefficient. The summary error statistics including the mean error, standard deviation of the error, and the R^2 are given at the end of the data section of the tables. The summary statistics in both Tables 5 and 6 indicate that the gust factor at a height of 10 m is best modeled when the sea-surface drag coefficient is modeled using the Large and Pond (1981) model with a cap of 0.0019.

Table 5. Quantitative Comparisons of Model and Observed Gust Factors, G(5,3600), at a Height of 44.9 m. Observed Gust Factors Are From Passage From C-MANs DSLN7, FPSN7, and FWYF1 and Are Computed Using a 10-Min Mean Wind Speed.

Data from C-MANs		C_d (L&P, 0.0019)		C_d (L&P, 0.0023)		C_d (Liu et al., 2012)	
U(44.9,600)[1]	G(5,600)[2]	G(5,3600)[3]	Error	G(5,3600)[3]	Error	G(5,3600)[3]	Error
12.4	1.24	1.21	-0.030	1.21	-0.030	1.21	-0.025
17.2	1.25	1.25	-0.003	1.25	-0.003	1.24	-0.006
22.4	1.26	1.28	0.015	1.28	0.015	1.27	0.007
27.1	1.31	1.29	-0.013	1.30	-0.007	1.29	-0.020
32.4	1.28	1.30	0.022	1.32	0.045	1.30	0.027
36.8	1.30	1.30	0.004	1.32	0.029	1.31	0.018
43.1	1.25	1.30	0.047	1.33	0.072	1.31	0.060
48.5	1.36	1.30	-0.056	1.33	-0.032	1.30	-0.058
56.4	1.34	1.30	-0.035	1.33	-0.012	1.29	-0.054
Mean	1.288	1.28	-0.002	1.298	0.011	1.28	0.000
Std. Dev.	0.042	0.034	0.032	0.044	0.035	0.035	0.038
R^2			0.429		0.320		0.170

[1] U(44.9,600) = Mean wind speed at a height of 44.9 m averaged over a period of 600 seconds

[2] G(5,600) = Maximum observed 5-s peak gust recorded during a 600-s period divided by the mean wind speed averaged over 600 seconds

[3] G(5,3600) = Modeled 5-s peak gust divided by the 3,600-s mean wind speed

Note: L&P = Large and Pond (1981)

Table 6. Quantitative Comparisons of Model and Observed Gust Factors, G(5,3600), at a Height of 44.9 m. Observed Gust Factors Are From Passage From C-MANs DSLN7, FPSN7, and FWYF1 and Are Computed Using a 30-Min Mean Wind Speed.

Data from C-MANs		C_d (L&P, 0.0019)		C_d (L&P, 0.0023)		C_d (Liu et al., 2012)	
U(44.9,600)[1]	G(5,600)[2]	G(5,3600)[3]	Error	G(5,3600)[3]	Error	G(5,3600)[3]	Error
12.4	1.24	1.21	-0.036	1.21	-0.036	1.21	-0.031
17.2	1.24	1.25	0.007	1.25	0.007	1.24	0.004
22.2	1.26	1.28	0.017	1.28	0.017	1.27	0.009
27.0	1.31	1.29	-0.018	1.30	-0.012	1.29	-0.026
32.3	1.27	1.30	0.023	1.32	0.047	1.30	0.029
36.4	1.31	1.30	-0.008	1.32	0.017	1.31	0.006
42.3	1.25	1.30	0.054	1.33	0.079	1.31	0.068
48.6	1.36	1.30	-0.052	1.33	-0.028	1.30	-0.054
Mean	1.28	1.28	-0.002	1.29	0.011	1.28	0.001
Std. Dev.	0.042	0.035	0.034	0.045	0.038	0.037	0.038
R^2			0.321		0.157		0.167

[1] U(44.9,600) = Mean wind speed at a height of 44.9 m averaged over a period of 600 seconds

[2] G(5,600) = Maximum observed 5-s peak gust recorded during a 600-s period divided by the mean wind speed averaged over 600 seconds

[3] G(5,3600) = Modeled 5-second peak gust divided by the 3,600-s mean wind speed

Note: L&P = Large and Pond (1981)

Buoy Gust Factors. Summaries of the gust factors from the buoy stations are presented in Table 7 and Table 8, where the mean and standard deviation of the gust factor are provided as well as the number of samples in each wind speed bin. As in the case of the gust factors from the C-MAN stations, the difference in the estimates of the gust factor computed using the 10-min or 30-min mean wind speeds is small, with a maximum difference of about 2% and an average difference of 0.2%, again suggesting that the use of the 10-min mean wind speed within which the hourly peak gust wind speed was recorded is representative of G(5,3600). There are only six 10-min mean wind speeds greater than 40 m/s and eight 30-min mean wind speeds greater than 40 m/s.

Table 7. Five-S Gust Factors From NOAA 10-m Discus Buoys. Measured Gust Factors Computed Using a 10-Min Mean Wind Speed.

U(10,600) (m/s)	G(5,3600)	Std. Dev. (m/s)	N
17.0	1.31	0.079	200
22.1	1.32	0.069	95
27.0	1.32	0.044	57
32.5	1.27	0.087	2
37.7	1.31	0.091	4
41.6	1.38	0.046	3
46.6	1.37	0.038	3

Table 8. Five-S Gust Factors From NOAA 10-m Discus Buoys. Measured Gust Factors Computed Using a 30-Min Mean Wind Speed.

U(10,1800) (m/s)	G(5,3600)	Std. Dev. (m/s)	N
17.0	1.33	0.080	212
22.2	1.33	0.068	90
27.0	1.33	0.038	50
32.3	1.28	0.062	2
36.3	1.28	0.151	2
41.2	1.36	0.063	6
47.7	1.38	0.004	2

Figure 17 and Figure 18 present gust factors computed from wind speed data obtained from the C-MAN stations during hurricanes along with the gust factors computed using the capped Large and Pond (1981) representation of the drag coefficient as well as the drag coefficient described in Liu et al. (2012).

Summary statistics are provided in Table 9 and Table 10, where it is seen that $C_{d_{10}}$ modeled using the Liu et al. (2012) model performs the worst and that the Large and Pond (1981) formulation with a cap of 0.0019 performs the best but still yields a negative R^2. The poor performance of all the models is because the observed gust factors for wind speeds between 30 m/s and 40 m/s are the lowest of all seven gust factors for either wind speed averaging duration.

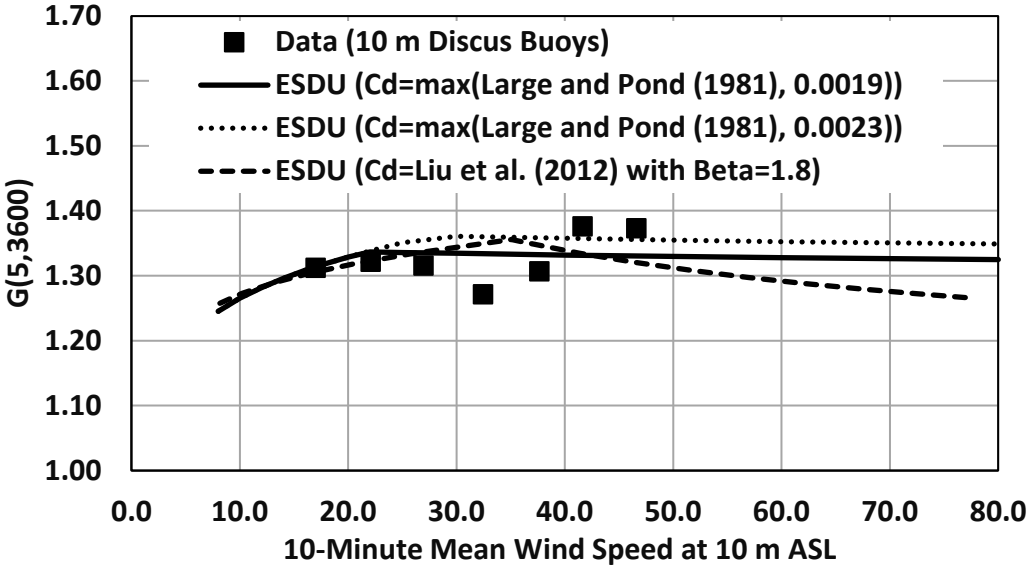

Figure 17. Modeled and measured gust factors at a height of 10.0 m. Measured gust factors from 10-m NOAA discus buoys, based on a 10-min mean wind speed.

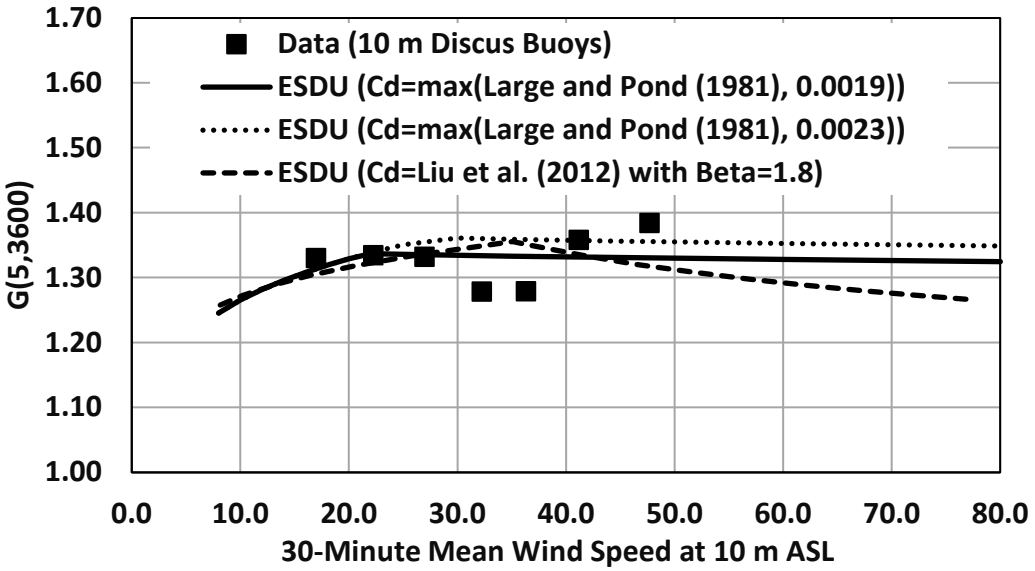

Figure 18. Modeled and measured gust factors at a height of 10.0 m. Measured gust factors from 10-m NOAA discus buoys, based on a 30-min mean wind speed.

Table 9. Quantitative Comparisons of Model and Observed Gust Factors, G(5,3600), at a Height of 44.9 m. Observed Gust Factors Are From Passage From C-MANs DSLN7, FPSN7, and FWYF1 and Are Computed Using a 10-Min Mean Wind Speed.

Data from C-MANs		C_d (L&P, 0.0019)		C_d (L&P, 0.0023)		C_d (Liu et al., 2012)	
U(44.9,600)	G(5,600)	G(5,3600)	Error	G(5,3600)	Error	G(5,3600)	Error
17.0	1.31	1.31	0.001	1.31	0.001	1.31	-0.005
22.1	1.32	1.34	0.015	1.34	0.017	1.33	0.004
27.0	1.32	1.34	0.020	1.36	0.043	1.34	0.023
32.5	1.27	1.33	0.062	1.36	0.088	1.35	0.080
37.7	1.31	1.33	0.026	1.36	0.051	1.34	0.038
41.6	1.38	1.33	-0.045	1.36	-0.019	1.33	-0.046
46.6	1.37	1.33	-0.043	1.36	-0.018	1.31	-0.059
Mean	1.33	1.33	0.002	1.35	0.021	1.33	0.002
Std. Dev.	0.039	0.008	0.040	0.017	0.044	0.016	0.051
R^2			-0.086		-0.303		-0.629

Note: L&P = Large and Pond (1981)

Table 10. Quantitative Comparisons of Model and Observed Gust Factors, G(5,3600), at a Height of 44.9 m. Observed Gust Factors Are From Passage From C-MANs DSLN7, FPSN7, and FWYF1 and Are Computed Using a 30-Min Mean Wind Speed.

Data from C-MANs		C_d (L&P, 0.0019)		C_d (L&P, 0.0023)		C_d (Liu et al., 2012)	
U(44.9,600)	G(5,600)	G(5,3600)	Error	G(5,3600)	Error	G(5,3600)	Error
17.0	1.31	1.31	0.001	1.31	0.001	1.31	-0.005
22.1	1.32	1.34	0.015	1.34	0.017	1.33	0.004
27.0	1.32	1.34	0.020	1.36	0.043	1.34	0.023
32.5	1.27	1.33	0.062	1.36	0.088	1.35	0.080
37.7	1.31	1.33	0.026	1.36	0.051	1.34	0.038
41.6	1.38	1.33	-0.045	1.36	-0.019	1.33	-0.046
Mean	1.33	1.33	0.005	1.35	0.023	1.33	0.005
Std. Dev.	0.037	0.008	0.038	0.017	0.040	0.016	0.048
R^2			-0.046		-0.120		-0.755

Note: L&P = Large and Pond (1981)

2.3 Drag Coefficient Summary

The review of the literature pertaining to the behavior of sea surface drag coefficients as a function of wind speed in hurricanes, coupled with the analysis of gust factors over the ocean in hurricanes, leads to somewhat ambiguous conclusions. Results of laboratory studies suggest that the drag coefficient reaches a maximum value and then remains constant with increasing wind speed. These experimental data suggest a maximum $C_{d_{10}}$ somewhere between 2×10^{-3} and 3×10^{-3}.

The gust factor analysis using NOAA data suggests that the drag coefficient does not reach a maximum at around 33 m/s as suggested in Powell et al. (2003) and, by extension, suggests that the drag coefficient is perhaps limited by the action of sea spray but does not decrease—at least for mean wind speeds at 10 m of up to approximately 50 m/s. The analysis of gust factors derived from the NOAA platforms suggests that the model for the sea surface drag coefficient capped at 0.0019 provides the best description of $C_{d_{10}}$. The gust factor data described in He et al. (2022) suggest that $C_{d_{10}}$ does decrease in high winds, but the winds used in their gust factor analysis may have been influenced by the effects of topography brought about by the small island on which the 6.5-m-tall anemometer mast was mounted.

Considering the suggestion of Smith and Montgomery (2014) that the flux-profile method may not be valid near the eyewall and consequently that the flux-profile approach leads to an underestimate of the true value of $C_{d_{10}}$, a model for $C_{d_{10}}$ having a maximum value—but not decreasing as the wind speed is increased—appears to be the most appropriate approach. However, because the mean profiles derived from the dropsondes at high wind speeds appear to be flatter, having a shape consistent with a low $C_{d_{10}}$, it is possible that the hurricane boundary model used herein underestimates the mean wind speeds at a height of 10 m but yields good estimates of gust factors.

As implied in the previous sections, there is no direct method to measure the sea surface drag coefficient; therefore, indirect methods are used. Currently, there is no consensus on which of the methods discussed herein yields the most reliable solutions, and there is still significant uncertainty about the behavior of $C_{d_{10}}$at very high (ultimate design) wind speeds, which for the most part occur near the eyewall of hurricanes.

Assuming that the boundary layer model used herein is valid, the relationship between the maximum 1-min wind speeds at the Saffir-Simpson hurricane category break points and wind speeds associated with other average times at heights of 10 m and 150 m above sea level is given in Table 11 and Table 12. IEC 61400-1 (IEC TC88-MT1 2019) defines the reference wind speed as a 10-min average wind speed with a return period of 50 years at turbine hub height. The reference wind speed values for Class 1A and Typhoon Class are provided in Table 1 of IEC 61400-1 as 111.9 and 127.5 miles per hour (mph) (50 and 57 m/s), respectively. According to Table 11 and Table 12 and assuming a hub height of 150 m, the Class 1A reference wind speed would be associated with the lower limit of a Category 2 hurricane, and the Typhoon Class reference wind speed would be associated with just under the lower limit of a Category 3 hurricane. The IEC 3-s extreme gust criteria, which are 70 m/s for Class 1A turbines and 80 m/s for Typhoon Class turbines, would be associated with a strong Category 2 and a moderate Category 3 hurricane, respectively.

Here, for simplicity, and based largely on the gust factor comparisons and the drag coefficient data presented in Figure 12, we suggest that the hurricane boundary layer be modeled using a mean profile described using the log law as given in Eq. 12 and a drag coefficient model that uses the Large and Pond (1981) model with an upper limit of 0.0019. This model for $C_{d_{10}}$results in a relatively low $C_{d_{10}}$ at high wind speeds but does not yield a reduction in $C_{d_{10}}$. The model is possibly conservative; however, until consensus on the behavior of $C_{d_{10}}$ at high wind speeds in

hurricanes is reached, we believe that this approach is prudent. The turbulence characteristics of the wind are well modeled using the ESDU (1982, 1983) models for atmospheric turbulence.

Table 11. Wind Speeds in m/s (mph) at the Break Points Between Hurricane Categories. Wind Speeds Are Given at Heights of 10 m and 150 m for Averaging Times of 1 Hour, 10 Minutes, 1 Minute, and 3 Seconds. Wind Speeds Are Computed Using a Sea Surface Drag Coefficient of 0.0019 and the ESDU (1982) Model for the Mean Boundary Layer.

	Category 1	Category 2	Category 3	Category 4	Category 5
Hourly, z=10 m	29.1 (65.2)	37.8 (84.6)	43.7 (97.2)	51.3 (114.7)	62.0 (138.6)
10 Minute, z=10	30.2 (67.6)	39.2 (87.7)	45.4 (101.5)	53.2 (118.9)	64.2 (143.7)
1 Minute, z=10 m	**33.1 (74.0)**	**42.9 (96.0)**	**49.6 (111.0)**	**58.1 (130.0)**	**70.2 (157.0)**
3-Second Gust, z=10 m	39.8 (89.0)	51.5 (115.3)	59.5 (133.2)	69.7 (155.9)	84.1 (188.1)
Hourly, z=150 m	37.7 (84.4)	49.0 (109.5)	56.7 (126.7)	66.4 (148.5)	80.2 (179.5)
10 Minute, z=150	38.9 (86.9)	50.5 (113.0)	58.5 (130.8)	68.6 (153.4)	82.9 (185.5)
1 Minute, z=150 m	42.0 (93.9)	54.8 (122.5)	63.5 (142.1)	74.6 (166.9)	90.4 (202.2)
3-Second Gust, z=150 m	47.2 (105.7)	61.9 (138.4)	71.9 (160.9)	84.7 (189.5)	102.9 (230.1)

Table 12. Wind Speeds in m/s (mph) at the Break Points Between Hurricane Categories. Wind Speeds Are Given at Heights of 10 m and 150 m for Averaging Times of 1 Hour, 10 Minutes, 1 Minute, and 3 Seconds. Wind Speeds Are Computed Using a Sea Surface Drag Coefficient of 0.0023 and the ESDU (1982) Model for the Mean Boundary Layer.

	Category 1	Category 2	Category 3	Category 4	Category 5
Hourly, z=10 m	28.9 (64.6)	37.5 (83.8)	43.4 (97.0)	50.8 (113.7)	61.4 (137.4)
10 Minute, z=10	30.0 (67.2))	39.0 (87.2)	45.1 (100.9)	52.8 (118.2)	63.8 (142.8)
1 Minute, z=10 m	**33.1 (74.0)**	**42.9 (96.0)**	**49.6 (111.0)**	**58.1 (130.0)**	**70.2 (157.0)**
3-Second Gust, z=10 m	40.2 (90.0)	52.1 (116.6)	60.2 (134.7)	70.5 (157.6)	85.0 (190.2)
Hourly, z=150 m	38.2 (85.5)	49.6 (111.0)	57.4 (128.5)	67.3 (150.6)	81.3 (182.0)
10 Minute, z=150	39.5 (88.3)	51.3 (114.9)	59.4 (133.0)	69.7 (155.9)	84.3 (188.6)
1 Minute, z=150 m	43.0 (96.2)	56.1 (125.5)	65.0 (145.5)	76.4 ((170.9)	92.5 (207.0)
3-Second Gust, z=150 m	48.9 (109.4)	64.0 (143.3)	74.4 (166.5)	87.6 (195.9)	106.3 (237.9)

3 Geospatial Risk Assessment

IEC 61400-1 (IEC TC88-MT1 2019) defines the reference wind speed as a 10-minute average wind speed with a return period of 50 years at turbine hub height. The reference wind speed values for Class 1A and Typhoon Class are provided in Table 1 of IEC 61400-1 as 111.9 and 127.5 mph (50 and 57 m/s), respectively.

Here, we estimated return periods associated with the IEC Class 1A and Typhoon Class limit-state hurricanes, using the methodology described in Section 1, on a nominal 10-km by 10-km grid covering the Gulf of Mexico offshore resource area as shown in Figure 19 and Figure 20, respectively. Hub height was assumed to be 150 m, which is typical for the 15-MW class turbines that may be deployed and is the hub height of the NREL 15-MW reference turbine (Gaertner et al. 2020). The wind speed at hub height is needed for comparison with the IEC 61400 design standards. The return period associated with the Class 1A limit state ranges from approximately 20 to 45 years whereas the return period associated with the Typhoon Class limit state ranges from approximately 40 to 110 years.

The 10-minute average wind speed with a return period of 50 years at turbine hub height obtained from the 500,000-year simulation is also presented on the same grid in Figure 21. The figure indicates that the reference wind speed across the Gulf of Mexico offshore wind resource area ranges from approximately 114 to 132 mph (51 to 59 m/s). Isoclines are also plotted corresponding to the IEC Class 1A and Typhoon Class design limit states. Note that no isocline for the Class 1A limit state appears on the plot of 50-year wind speeds because all 50-year wind speed values obtained from the simulation are greater than the Class 1A reference wind speed (111.9 mph, 50 m/s).

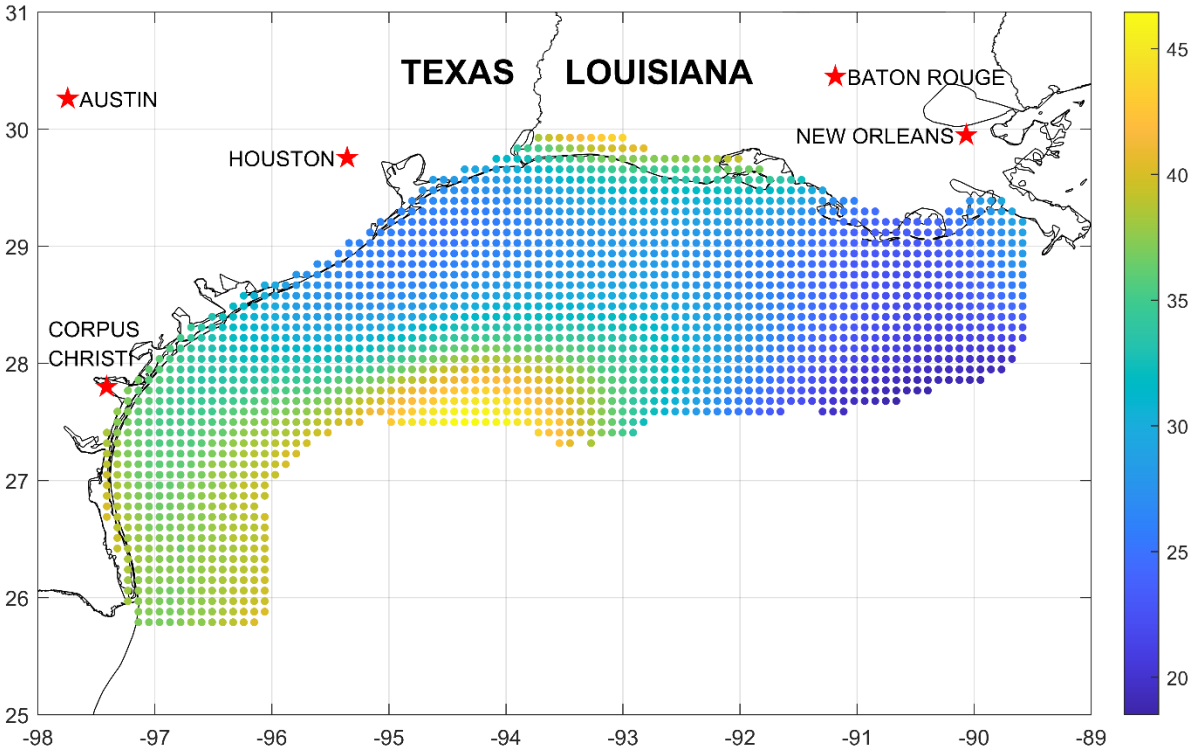

Figure 19. Return period (years) associated with the IEC Class 1A limit-state reference wind speed of 111.9 mph (50 m/s) obtained from a 500,000-year hurricane simulation.

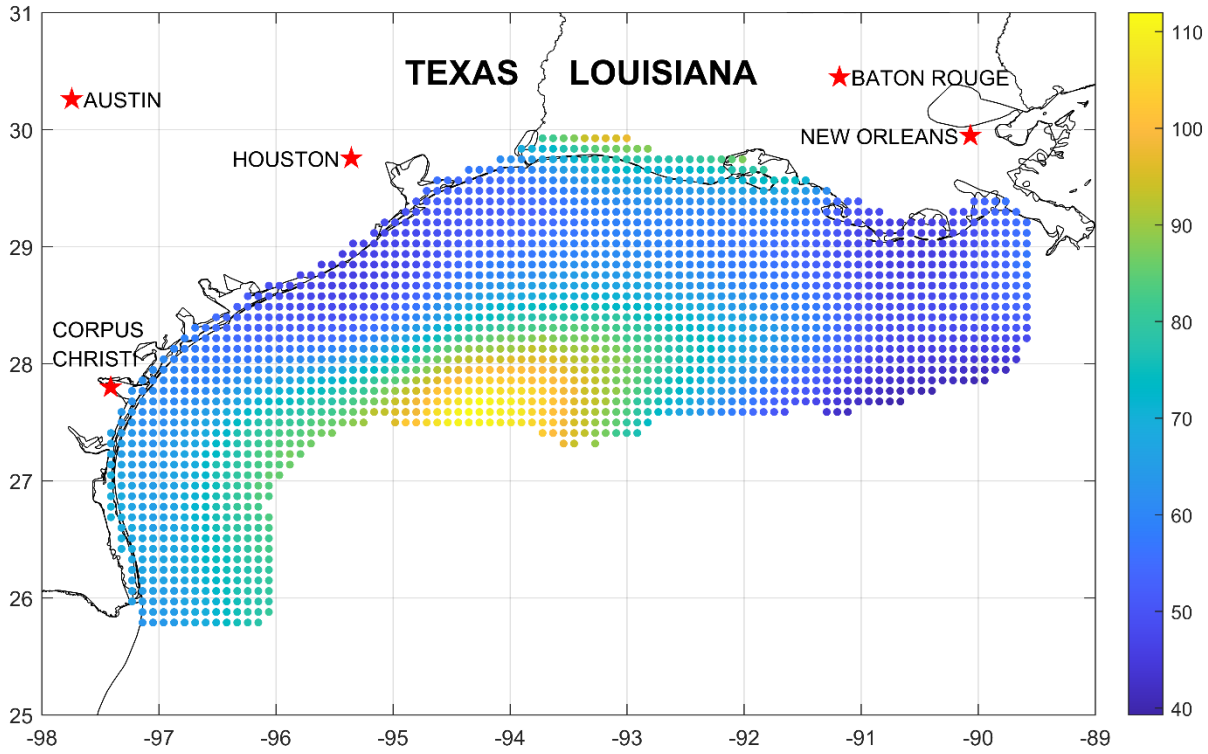

Figure 20. Return period (years) associated with the IEC Typhoon Class limit-state reference wind speed of 127.5 mph (57 m/s) obtained from a 500,000-year hurricane simulation

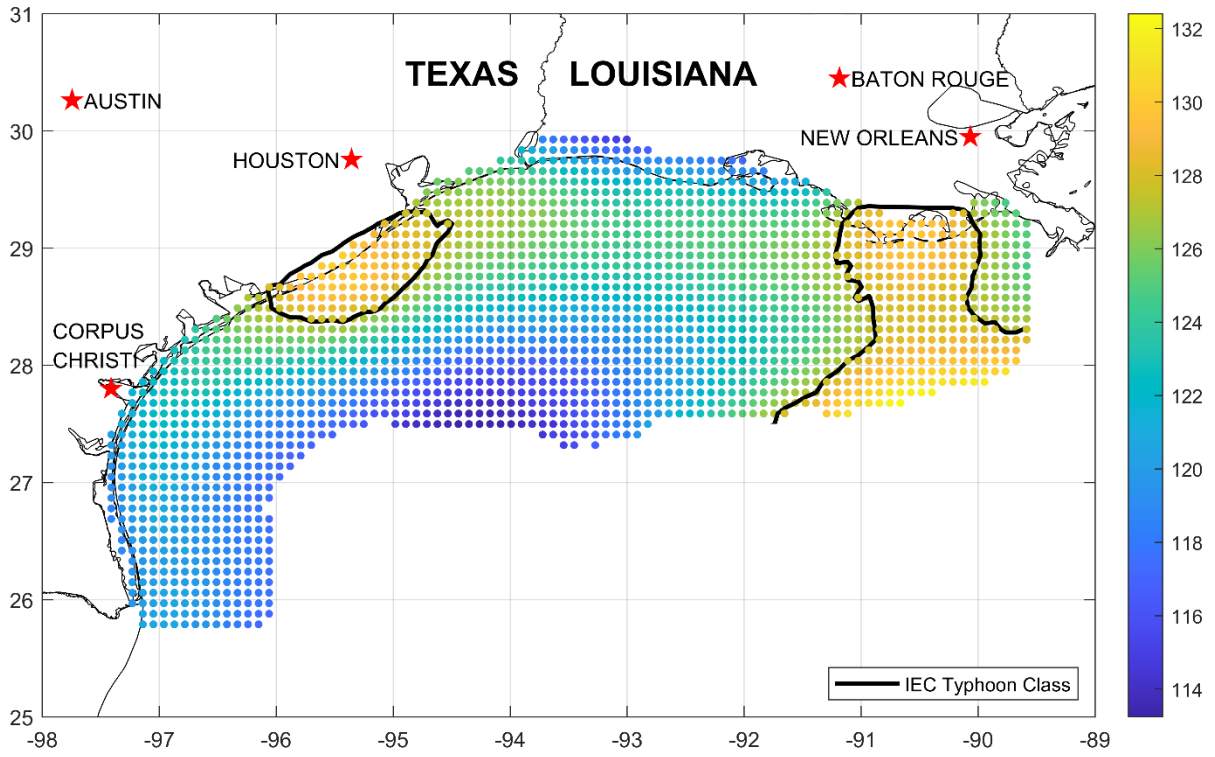

Figure 21. Ten-min sustained wind speed (mph) at 150 m with a return period of 50 years obtained from a 500,000-year hurricane simulation.

Note: No isocline for the Class 1A limit state appears because all simulated values of the 50-year wind speed are greater than the Class 1A reference wind speed (111.9 mph, 50 m/s).

4 Hazard Curves

Wind speed hazard curves have been generated on the same grid covering the Gulf of Mexico offshore wind resource area for return periods from 10 to 10,000 years. The wind speed hazard curves have been defined in terms of the 3-s gust and 10-min sustained wind speeds at 10-m elevation and as the 10-min sustained wind speed at hub height (assuming a hub height of 150 m). Hazard maps of the 10-min sustained wind speed at hub height are provided for return periods of 50, 100, 500, and 1,000 years in Figure 22 through Figure 25.

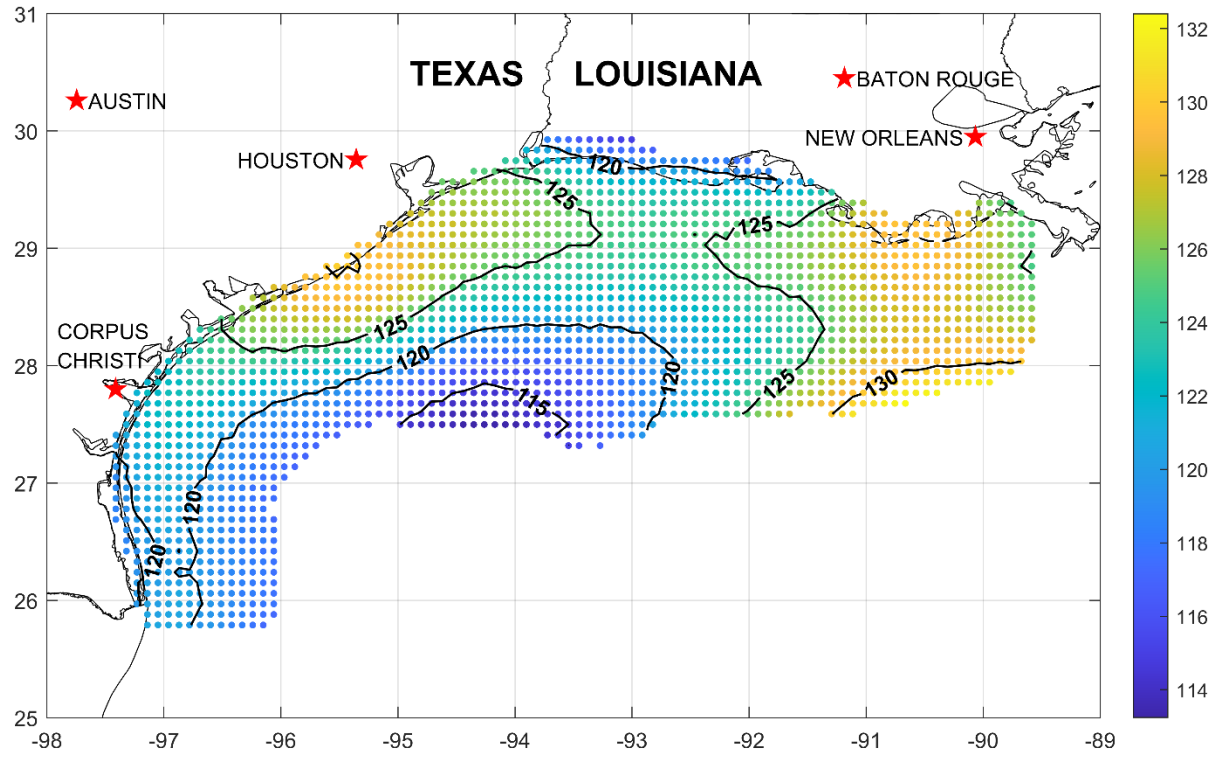

Figure 22. Ten-min sustained wind speed (mph) at 150-m height with a return period of 50 years obtained from a 500,000-year hurricane simulation

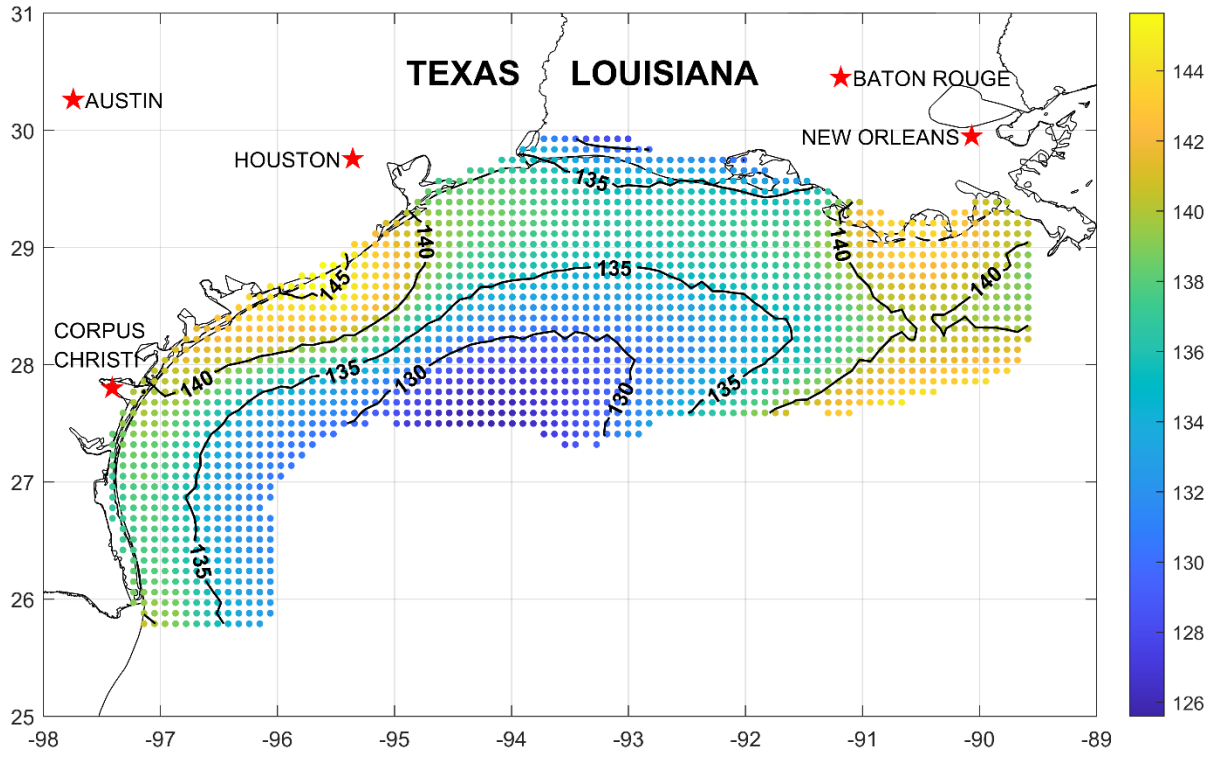

Figure 23. Ten-min sustained wind speed (mph) at 150-m height with a return period of 100 years obtained from a 500,000-year hurricane simulation.

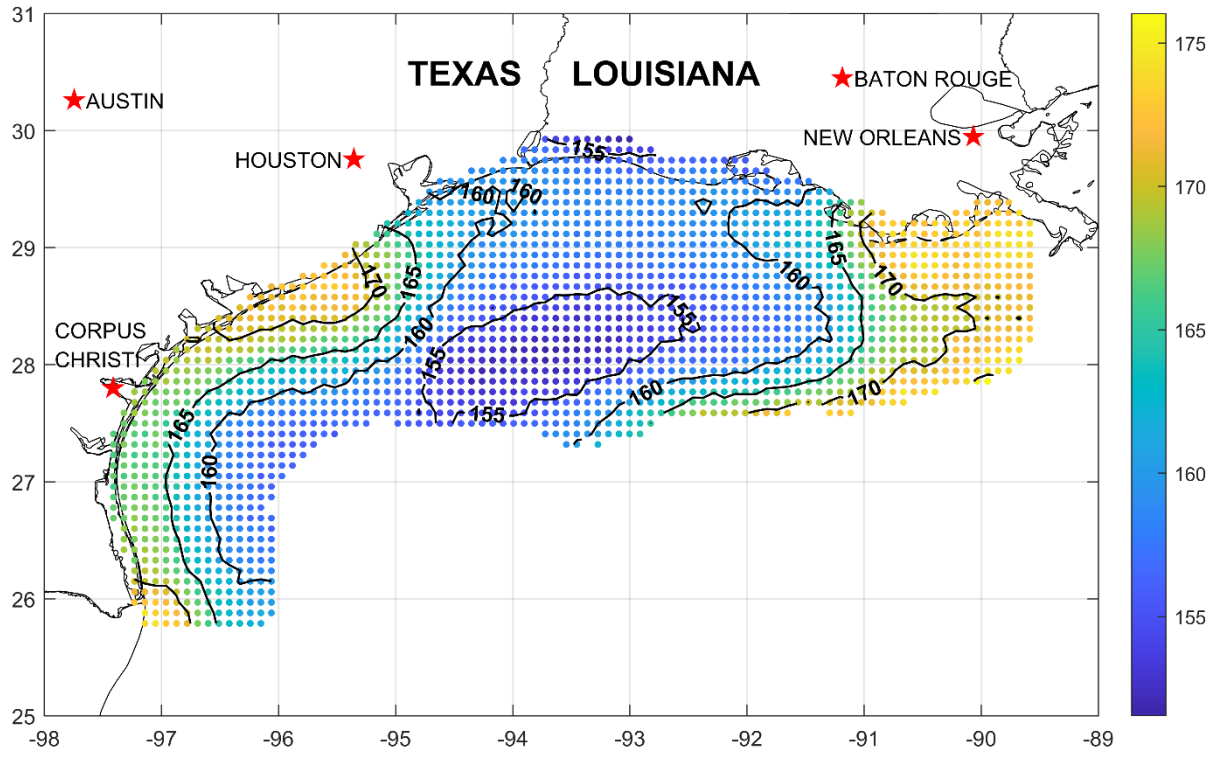

Figure 24. Ten-min sustained wind speed (mph) at 150-m height with a return period of 500 years obtained from a 500,000-year hurricane simulation

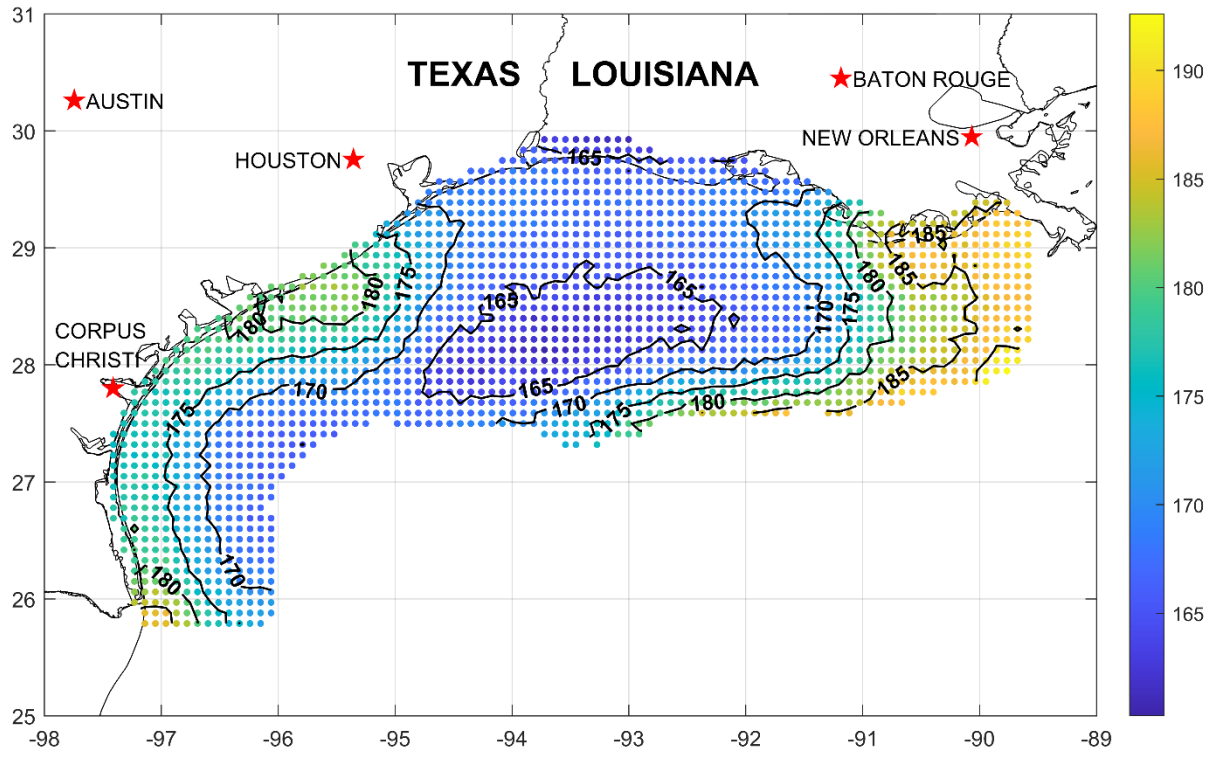

Figure 25. Ten-min sustained wind speed (mph) at 150-m height with a return period of 1,000 years obtained from a 500,000-year hurricane simulation

5 Summary

A challenge in relating a given hurricane event to the IEC design criteria stems from inconsistent hurricane wind speed terminology between the Saffir-Simpson hurricane scale, used by the National Hurricane Center to estimate the intensity of hurricanes, and IEC design criteria used for the design of turbines. Using the latest research on turbulence characteristics of the hurricane boundary layer, definitions of the Saffir-Simpson wind speed scale are provided in Section 2 for four averaging times (e.g., 3 seconds, 1 minute, 10 minutes, and 1 hour) and two heights (e.g., 10 m and 150 m). In the same section, definitions of the Class 1A and Typhoon Class limit states are provided in terms of an equivalent Saffir-Simpson category.

For the boundary layer model used, we compared the relationship between the maximum 1-min wind speeds at the Saffir-Simpson hurricane category break points at 10-m height and wind speeds associated with 3-s averaging times used by IEC wind turbine design standards at 150-m height. The 70-m/s 3-s gust for IEC Class 1A turbines was found to be associated with a strong Category 2 hurricane, and the 80-m/s 3-s gust for IEC Typhoon Class turbines was found to be associated with a moderate Category 3 hurricane.

Using the hurricane hazard model outlined in Section 1, the wind hazard for the Gulf of Mexico Offshore Wind Energy Call Area was defined on a grid with nominal resolution of 10 km. Results of the geospatial risk assessment are provided in Sections 3 and 4. Even though the IEC prescribes the reference wind speeds associated with Class 1A and Typhoon Class limit states to be 50 years, in Section 3 the return periods associated with the Class 1A limit state were found to range from approximately 20 to 45 years, while the return period associated with the Typhoon Class limit state ranges from approximately 40 to 110 years. This indicates that the Class 1A limit state may be nonconservative for the entire Gulf of Mexico Offshore Wind Energy area, while the Typhoon Class limit state may be adequate for the design of turbines in some regions of the Gulf of Mexico Offshore Wind Energy Call Area. In Section 4, maps of the 10-min mean wind speeds at 150-m height associated with return periods of 50 to 1,000 years are provided. The 50-year value was found to range from approximately 114 to 132 mph (51 to 59 m/s).

References

Andreas, E. L. 2004. "Spray Stress Revisited." *Journal of Physical Oceanography* 34, 1429–1440. https://doi.org/10.1175/1520-0485(2004)034<1429:SSR>2.0.CO;2

Blake, E. S., C. W. Landsea, and E. J. Gibney. 2011. "The deadliest, costliest, and most intense United States tropical cyclones from 1851 to 2010 (and other frequently requested hurricane facts)." NOAA Technical Memorandum NWS NHC-6, National Weather Service, National Hurricane Center, Miami, Florida, August, 47 pp. www.nhc.noaa.gov/pdf/nws-nhc-6.pdf.

Curcic, M. and B. K. Haus. 2020. Revised estimates of ocean surface drag in strong winds. Geophysical Research Letters, 47, e2020GL087647. https://doi.org/10.1029/2020GL087647.

DeMaria, M. and J. Kaplan 1999. "An updated Statistical Hurricane Intensity Prediction Scheme (SHIPS) for the Atlantic and Eastern North Pacific Basins." *Weather and Forecasting* 14: 326–337. https://doi.org/10.1175/1520-0434(1999)014<0326:AUSHIP>2.0.CO;2

Donelan, M. A. 2018. "On the decrease of the oceanic drag coefficient in high winds." *Journal of Geophysical Research: Oceans* 123: 1485–1501. https://doi.org/10.1002/2017JC013394.

Donelan, M. A., B. K. Haus, N. Reul, W. J. Plant, M. Stiassnie, H. C. Graber, O. B. Brown, and E. S. Saltzman. 2004. "On the limiting aerodynamic roughness of the ocean in very strong winds." *Geophys. Res. Lett.* 31, L18306. doi:10.1029/2004GL019460.

Emanuel, K. A. 1988. "The Maximum Intensity of Hurricanes." *Journal of the Atmospheric Sciences* 45: 1143–1155. https://doi.org/10.1175/1520-0469(1988)045<1143:TMIOH>2.0.CO;2

Emanuel, K. A, S. Ravela, E. Vivant, and C. Risi. 2006. "A statistical–deterministic approach to hurricane risk assessment." *Bull. Amer. Meteor. Soc.* 19: 299–314. https://doi.org/10.1175/BAMS-87-3-299

ESDU. 1982. "Strong Winds in the Atmospheric Boundary Layer, Part 1: Mean Hourly Wind Speed." Engineering Sciences Data Unit Item Number 82026, London, England.

ESDU. 1983. "Strong Winds in the Atmospheric Boundary Layer, Part 2: Discrete Gust Speeds." Engineering Sciences Data Unit Item Number 83045, London, England.

Fuchs, Rebecca, Walt Musial, Gabriel R. Zuckerman, Mayank Chetan, Melinda Marquis, Leonardo Rese, Aubryn Cooperman, Patrick Duffy, Rebecca Green, Philipp Beiter, Daniel Mulas Hernando, James A. Morris, Jr., Alyssa Randall, Jonathan A. Jossart, Lauren Mudd, Peter Vickery. 2023. *Assessment of Offshore Wind Energy Opportunities and Challenges in the U.S. Gulf of Mexico*. Golden, CO: National Renewable Energy Laboratory. NREL/TP-5000-88195. nrel.gov/docs/fy24osti/88195.pdf.

Gao, Z., S. Zhou, J. Zhang, Z. Zeng, and X. Bi. 2021. "Parameterization of sea surface drag coefficient for all wind regimes using 11 aircraft eddy-covariance measurement databases." *Atmosphere*, 12: 1485. https://doi.org/10.3390/atmos12111485.

Gaertner, Evan, Jennifer Rinker, Latha Sethuraman, Frederik Zahle, Benjamin Anderson, Garrett Barter, Nikhar Abbas, Fanzhong Meng, Pietro Bortolotti, Witold Skrzypinski, George Scott, Roland Feil, Henrik Bredmose, Katherine Dykes, Matt Shields, Christopher Allen, and Anthony Viselli. 2020. *Definition of the IEA Wind 15-Megawatt Offshore Reference Wind*. Golden, CO: National Renewable Energy Laboratory (NREL). NREL/TP-5000-75698. https://www.nrel.gov/docs/fy20osti/75698.pdf.

He, J. Y., Q. S. Li, and P. W. Chan. 2020. "Reduced gust factor for extreme tropical cyclone winds over ocean*." J. Wind Eng. Ind. Aerod.* 208: 2–9. https://doi.org/10.1016/j.jweia.2020.104445

Hock, T. R. and J. L. Franklin. 1999. "The NCAR GPS dropwindsonde." *Bull. Am. Meteorol. Soc.* 80: 407–420. https://doi.org/10.1175/1520-0477(1999)080<0407:TNGD>2.0.CO;2
Holland, G. J. 1980. "An analytic model of the wind and pressure profiles in hurricanes." *Mon. Wea. Rev.* 108: 1212–1218. https://doi.org/10.1175/1520-0493(1980)108<1212:AAMOTW>2.0.CO;2

Holland, G. J., J. I. Belanger, and A. Fritz. 2010. "A revised model for radial profiles of hurricane winds." *Mon. Weather Rev.* 138, 4393–4401. https://doi.org/10.1175/2010MWR3317.1

Holthuijsen, L. H., M. D. Powell, and J. D. Pietrzak. 2012. "Wind and waves in extreme hurricanes." *J. Geophys. Res.* 117: C09003. doi:10.1029/2012JC007983.

Hsu, J.-Y., R. Lien, E. A. D'Asaro, and T. B. Sanford. 2019. "Scaling of drag coefficients under five tropical cyclones." *Geophys. Res. Lett.* 46: 3349–3358. https://doi.org/10.1029/2018GL081574.

IEC TC88-MT1. 2019. *IEC 61400-1 Ed.4. Wind Energy Generation Systems. Part 1: Design Requirements.* International Electrotechnical Commission: Geneva, Switzerland.

Jarosz, E., D. A. Mitchell, D. W. Wang, and W. J. Teague. 2007. "Bottom-up determination of air-sea momentum exchange under a major tropical cyclone." *Science* 315: 1707–1709. doi: 10.1126/science.1136466.

Kepert, J. 2001. "The dynamics of boundary layer jets within the tropical cyclone core. Part I: Linear theory." *J. Atmos. Sci.* 58: 2469–2484. https://doi.org/10.1175/1520-0469(2001)058<2469:TDOBLJ>2.0.CO;2

Landsea, C. W. and J. L. Franklin. 2013. "Atlantic Hurricane Database Uncertainty and Presentation of a New Database Format." *Mon. Weather Rev.* 141: 3576–3592. https://doi.org/10.1175/MWR-D-12-00254.1

Large, W. G. and S. Pond. 1981. "Open Ocean Momentum Flux Measurements in Moderate to Strong Winds." *J. Phys. Oceanogr* 11: 324–336. https://doi.org/10.1175/1520-0485(1981)011<0324:OOMFMI>2.0.CO;2

Lee, W., S.-H. Kim, I.-L. Moon, M. M. Bell, and I. Ginis. 2022. "New parameterization of air-sea exchange coefficients and its impact on intensity prediction under major tropical cyclones." *Front. Mar. Sci.* 9: 1046511. doi: 10.3389/fmars.2022.1046511.

Liu, B., C. Guan, and L. Xie. 2012. "The wave state and sea spray related parameterization of wind stress applicable from low to extreme winds." *J. Geophys. Res.* 117: C00J22. doi:10.1029/2011JC00778.

Makin, V. K. 2005. "A note on the drag of the sea surface at hurricane winds." *Boundary-Layer Meteorology* 115: 169–176. https://doi.org/10.1007/s10546-004-3647-x

Musial, W., and T. Greco. 2020. "Feasibility of Ocean-Based Renewable Energy in the Gulf of Mexico." Marine Technology Society Journal 54(6): 9–23. https://doi.org/10.4031/MTSJ.54.6.3.

Peng, S. and Y. Li. 2015. "A parabolic model of drag coefficient for storm surge simulation in the South China Sea." *Sci. Rep.* 5: 15496. doi: 10.1038/srep15496.

Powell, M. D., P. J. Vickery, and T. A. Reinhold. 2003. "Reduced drag coefficient for high wind speeds in tropical cyclones." *Nature* 422: 279–283. doi:10.1038/nature01481.

Powell, M., G. Soukup, S. Cocke, S. Gulati, N. Morisseau-Leroy, S. Hamid, N. Dorst, and L. Axe. 2005. "State of Florida hurricane loss projection model: Atmospheric science component." *J. Wind Eng. Ind. Aerodyn.* 93: 651–674. https://doi.org/10.1016/j.jweia.2005.05.008

Rayner, N. A., D. E. Parker, E. B. Horton, C. K. Folland, L. V. Alexander, D. P. Rowell, E. C. Kent, and A. Kaplan. 2003. "Global analyses of sea surface temperature, sea ice, and night marine air temperature since the late nineteenth century." *Journal of Geophysical Research* 108(D14): 4407. 10.1029/2002JD002670.

Richter, D. H., R. Bohac, and D. P. Stern. 2016. "An assessment of the flux Profile method for determining air–sea momentum and enthalpy fluxes from dropsonde data in tropical cyclones." *J. Atmos. Sci.* 73: 2665–2682. doi:10.1175/JAS-D-15-0331.1.

Richter, D. H., C. Wainwright, D. P. Stern, G. H. Bryan, and D. Chavas. 2021. "Potential low bias in high-wind drag coefficient inferred from dropsonde data in hurricanes." *J. Atmos. Sci.* 78: 2339–2352.

Shi, J., Z. Zhong, X. Li, G. Jiang, W. Zeng, and Y. Li. 2016. "The Influence of wave state and sea spray on drag coefficient from low to high wind speeds." *Journal of Ocean University of China* 15: 41–49. doi: 10.1007/s11802-016-2655-z.

Smith, R. K. and M. T. Montgomery. 2010. "Hurricane boundary-layer theory." *Q. J. R. Meteorol. Soc.* 136: 1665–1670. doi:10.1002/qj.679.

Smith R. K. and M. T. Montgomery. 2014. "On the existence of the logarithmic surface layer in the inner core of hurricanes." *Quart. J. Roy. Meteor. Soc.* 140: 72–81. https://doi.org/10.1002/qj.2121.

Takagaki, N., S. Komori, N. Suzuki, K. Iwano, T. Kuramoto, S. Shimada, R. Kurose, and K. Takahashi. 2012. "Strong correlation between the drag coefficient and the shape of the wind sea spectrum over a broad range of wind speeds." *Geophys. Res. Lett.* 39: L23604. doi:10.1029/2012GL053988.

Thompson, E. F. and V. J. Cardone. 1996. "Practical Modeling of Hurricane Surface Wind Fields." *J. Wtrwy., Port, Coast., and Oc. Engrg.* 122: 195–205.

Troitskaya, Y. I., D. A. Sergeev, A. A. Kandaurov, G. A. Baidakov, M. A. Vdovin, and V. I. Kazakov. 2012. "Laboratory and theoretical modeling of air-sea momentum transfer under severe wind conditions." *J. Geophys. Res.* 117: C00J21. doi:10.1029/2011JC007778.

Vickers, D., L. Mahrt, and E. L. Andreas. 2013. "Estimates of the 10-m neutral sea surface drag coefficient from aircraft eddy-covariance measurements." *J. Phys. Oceanogr.* 43(2): 301–310. https://doi.org/10.1175/JPO-D-12-0101.1

Vickery, P. J., P. F. Skerlj, A. C. Steckley, and L. A. Twisdale. 2000a. "Hurricane Wind Field Model for Use in Hurricane Simulations." *J. Struct. Engrg.* 10: 1203–1221. https://doi.org/10.1061/(ASCE)0733-9445(2000)126:10(1203)

Vickery, P. J., P. F. Skerlj, and L. A. Twisdale, Jr. 2000b. "Simulation of Hurricane Risk in the U.S. Using an Empirical Track Model." *J. Struct. Engrg. , ASCE* 126(). 1222–1237. https://doi.org/10.1061/(ASCE)0733-9445(2000)126:10(1222)

Vickery, P. J. 2005. "Simple Empirical Models for Estimating the Increase in the Central Pressure of Tropical Cyclones after Landfall along the Coastline of the United States." *J. Appl. Meteor.* 44: 1807–1826.. https://doi.org/10.1175/JAM2310.1

Vickery, P. J. and P. F. Skerlj. 2005. "Hurricane Gust Factors Revisited." *J. Struct. Engrg.* 131(): 825–832, https://doi.org/10.1061/(ASCE)0733-9445(2005)131:5(825)

Vickery, P. J. and D. Wadhera. 2008. "Statistical Models of Holland Pressure Profile Parameter and Radius to Maximum Winds of Hurricanes from Flight Level Pressure and H*Wind Data." *J. Appl. Meteor.* 47: 2497–2517, https://doi.org/10.1175/2008JAMC1837.1

Vickery, P. J., D. Wadhera, M. D. Powell, and Y. Chen. 2009a. "A hurricane boundary layer and wind field model for use in engineering applications." *J. Appl. Meteor.*. 48: 381–405. https://doi.org/10.1175/2008JAMC1841.1.

Vickery, P. J., D. Wadhera, L. A. Twisdale, and F. M. Lavelle. 2009b. "United States Hurricane Wind Speed Risk and Uncertainty." *J. Struct. Engrg.* 135: 301–320, https://doi.org/10.1061/(ASCE)0733-9445(2009)135:3(301)

Ye, L., Y. Li, and Z. Gao. 2022. "Surface layer drag coefficient at different radius ranges in tropical cyclones." *Atmosphere* 13: 280. https://doi.org/10.3390/atmos13020280.

Zou, Z., D. Zhao, J. Tian, B. Liu, and J. Huang. 2018. “Drag coefficients derived from ocean current and temperature profiles at high wind speeds.” *Tellus A: Dynamic Meteorology and Oceanography* 70(1): 1–13, doi: 10.1080/16000870.2018.1463805.

Appendix. Hurricane Wind Speed Boundary Layer Model

The mean wind speed as a function of height is described using

$$U(z) = \frac{u_*}{k}\left[\ln\left(\frac{z}{z_0}\right) - 0.5\left(\frac{z}{H}\right)^2\right] \tag{24}$$

where u_* is the friction velocity, z is height above ground, z_0 is the aerodynamic roughness length, k is the von Karman constant, taken as 0.4, and H is the height of the boundary layer.

The boundary layer height for winds over water is computed from

$$H = 385 + \frac{0.291}{I} \tag{25}$$

where I is the inertial stability parameter defined as

$$I = \sqrt{\left(f + \frac{2V}{r}\right)\left(f + \frac{V}{r} + \frac{\partial V}{\partial r}\right)} \tag{26}$$

where f is the Coriolis parameter, V is the mean wind speed, and r is the distance from the center of the storm. As noted in Vickery et al. (2009a), the $\frac{\partial \mathrm{V}}{\partial \mathrm{r}}$ term in Eq. 26 is ignored. Because H is inversely proportional to I, the boundary layer height decreases with increasing wind speed and decreasing distance from the center of the storm. In the computation of I, r is constrained to be greater than radius of maximum wind (RMW).

The ratio of the mean over water surface level (10-meter [m]) wind speed to the mean wind speed at the top of the boundary layer obtained from the model varies between about 0.67 and 0.74, with 0.71 being a representative value. Figure 26 compares the variation of wind speed with height derived from Eq. 24 through 26 to the profiles derived from dropsonde analyses. The model profiles are computed with the only input being the maximum wind speed within the boundary layer (i.e., a direct output of the numerical solution of the equations of motion of a translating hurricane as described in Vickery et al. (2009a, 2000a) or Thompson and Cardone (1996). The agreement between the modeled and measured profiles is seen to be good.

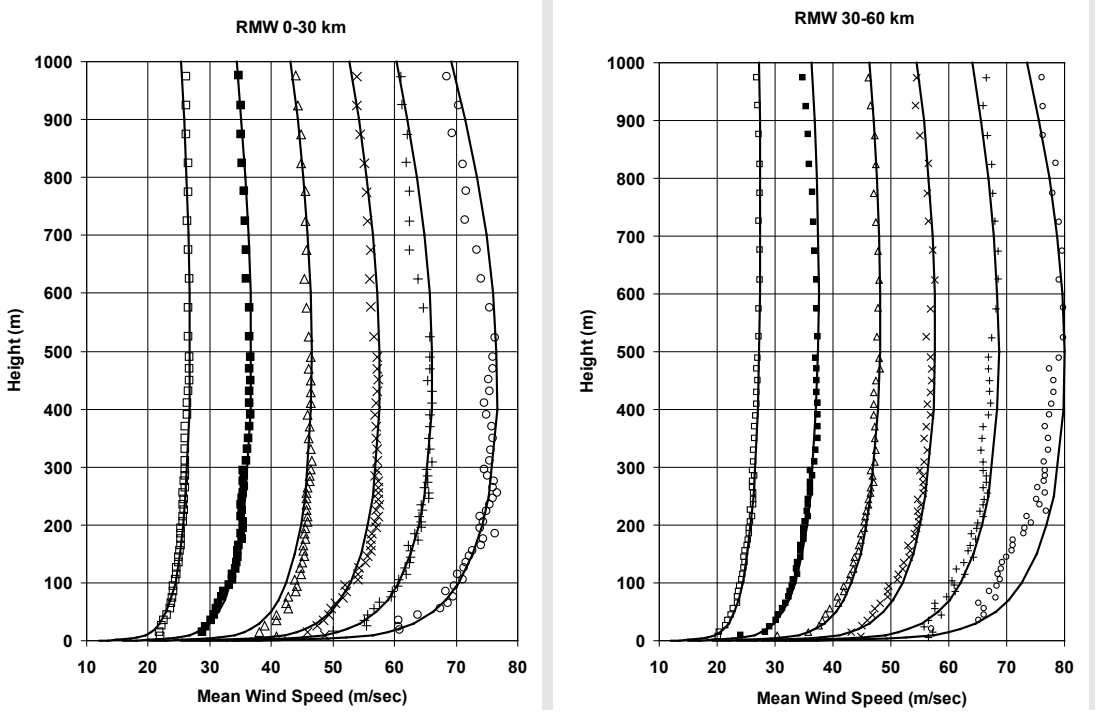

Figure 26. Comparisons of modeled and observed variation of wind speed with height (over water) in hurricanes. Observed data from dropsondes.

The parameter, z_0, is responsible for the near-surface variation of the mean wind speed with height (Eq. 24) and is also responsible for the near-surface turbulence (Vickery and Skerlj, 2005) in hurricanes. To estimate z_0, Eq. 24 is used, and ignoring the higher order term in z, which is negligible near the surface, and rearranging, results in u_* being defined as

$$u_* = \frac{k \cdot U(3600, z)}{\ln\left(\frac{z}{z_0}\right)} \tag{27}$$

where $U(3600, z)$ is the mean wind speed averaged over a period of 1 hour (3,600 seconds).

In a marine environment, z_0 varies with the mean wind speed (because the sea surface drag coefficient varies with the mean wind speed). The sea surface drag coefficient, $C_{d_{10}}$, is related to the aerodynamic roughness, z_0, through the surface shear stress, τ_0. The surface shear stress is defined as

$$u_* = \frac{k \cdot U(3600, z)}{\ln\left(\frac{z}{z_0}\right)} \tag{28}$$

Combining Eq. 24, 27, and 28 yields

$$z_0 = 10\exp\left[-k/\sqrt{C_{d_{10}}}\right] \tag{29}$$

The marine boundary layer, $C_{d_{10}}$, is computed using the wind speed limited representation of $C_{d_{10}}$ described in Vickery et al. (2009a), where:

$$C_{d_{10}} = (0.49 + 0.065|U(3600,10)|)10^{-3}; \qquad C_{d_{10}} \leq C_{d_{max}} \tag{30}$$

Equation 30 is a capped representation of the drag coefficient described in Large and Pond (1981).

The limiting value of $C_{d_{max}}$ is modeled as a function of the distance from the center of storm using the models presented in Vickery et al. (2009a). The limiting value $C_{d_{max}}$ given in Vickery et al. (2009a) is described using

$$C_{d_{max}} = (0.0881r + 17.66)10^{-4}; \quad 0.0019 \leq C_{D_{max}} \leq 0.0025 \tag{31}$$

In Eq. 31, *r* is the distance from the storm center in kilometers (km). The value of $C_{d_{max}}$ given in Eq. 31 is reached at hourly mean wind speeds near 22 meters per second (m/s) for small storms (RMW 20 km to 30 km) and 30 m/s for large storms (RMW 60 km to 100 km). Given the mean wind speed at 10 m, Eq. 27 through 29 are used to compute the surface roughness. Given the surface roughness length and the mean wind speed at 10 m, gust factors, turbulence intensities, and so on are readily computed.